

# NONPERTURBATIVE QCD WITH MODERN TOOLS

C. D. ROBERTS

*Physics Division, Bldg. 203, Argonne National Laboratory  
Argonne IL 60439-4843, USA*

In these lectures I introduce and explore a range of topics of contemporary interest in hadronic physics: from what drives the formation of a nonzero quark condensate to the effect that mechanism has on light and heavy meson form factors, and the properties of the quark-gluon plasma. The trail leads naturally through a discussion of confinement, dynamical chiral symmetry breaking and bound state structure: phenomena that require nonperturbative methods for their explanation. In all of this, the necessary momentum-dependent modification of the quark and gluon propagators plays a significant role.

## 1 Hadron Physics

The strong interaction spectrum has a regularity that can be understood simply. Mesons are composed of a constituent quark and its antiparticle, and baryons of three constituent quarks. The quarks have quantum numbers: colour - red, blue, green; flavour - up, down, strange, etc., and spin - up or down. Attributing a flavour-dependent mass to these constituent quarks:  $M_u \approx M_d \sim 320$  MeV,  $M_s \sim 400$  MeV, and demanding that only colour singlets exist, one obtains a quantitative description that includes the multiplet structure. Almost.

In this picture the pion is a pseudoscalar meson with the spins of its constituents antiparallel:  $m_\pi \approx 140$  MeV. Align the spins and one has a vector meson, which is identified with the  $\rho$ :  $m_\rho \approx 770$  MeV. The simplest explanation of the mass ratio in Eq. (1)<sup>1</sup>

$$\left. \begin{array}{l} \frac{m_\rho^2}{m_\pi^2} = 30 \\ \frac{m_{a_1}^2}{m_{a_0}^2} = 1.7 \end{array} \right| \left. \begin{array}{l} \frac{m_{\pi'}^2}{m_\pi^2} = 86 \\ \frac{m_{\rho'}^2}{m_\rho^2} = 3.5 \end{array} \right| \left. \begin{array}{l} \frac{m_N^2}{m_\pi^2} = 45 \\ \frac{m_N^2}{m_\rho^2} = 1.5 \end{array} \right| \quad (1)$$

is hyperfine splitting, akin to the splitting of each level in the hydrogen atom that measures whether the spin of the electron and proton are aligned or not. A difficulty with this interpretation, however, is that the pseudovector- to scalar-meson mass ratio,  $m_{a_1}^2/m_{a_0}^2$ , should have the same origin but it is much smaller. Equation (1) also shows that the excitation energy in the pseudoscalar channel, which is measured by the mass difference between the pion and its

first excited state, is much larger than that in the vector channel. As a final illustration of the peculiarity of the pion, I note that the expected value of the ratio in the third column is  $\approx 2$  because it should just count the number of constituents in a baryon as compared to a meson. It is for the  $\rho$  but not for the  $\pi$ . The “unnaturally” low mass of the  $\pi$  has many consequences; e.g., it means that attraction in the  $N$ - $N$  interaction persists over a much longer range than repulsion, which underlies the line of nuclear stability and makes possible the existence of heavy elements.

Although the  $\pi$  was the first meson discovered, its peculiar properties are still not understood widely. They are almost completely determined by the phenomena driving dynamical chiral symmetry breaking [DCSB]. That is an intrinsically nonperturbative effect, the understanding of which is one focus of these lecture notes.

Quarks provide a means of understanding much of the regularity in the hadron spectrum. However, they do not form part of that spectrum: quarks carry the colour quantum number and the spectrum consists only of colourless objects. Are they then a mathematical artifice useful only as a means of realising group theory? No, they are observed in inclusive, deep inelastic scattering:  $e p \rightarrow e' + \text{“debris”}$ , even though the debris never contains an isolated quark.

The cross section for deep inelastic scattering from a proton target is

$$\frac{d^2\sigma}{dQ^2 d\nu} = \frac{\alpha^2}{4E_e^2 \sin^4 \frac{\theta}{2}} \left( 2W_1(Q^2, \nu) \sin^2 \frac{\theta}{2} + W_2(Q^2, \nu) \cos^2 \frac{\theta}{2} \right), \quad (2)$$

where  $\theta$  is the scattering angle,  $Q^2$  is the spacelike squared momentum transfer, and  $\nu = E_{e'} - E_e$  for  $\vec{p}_p = 0$ . It is characterised by two scalar functions:  $W_1$ ,  $W_2$ , which contain a great deal of information about proton structure. If the proton is a composite particle composed of pointlike constituents, then it follows that for  $Q^2 \rightarrow \infty, \nu \rightarrow \infty$  with  $\nu \gg Q^2$

$$\begin{aligned} W_1(Q^2, \nu^2) &\rightarrow F_1(Q^2/\nu^2), \\ \nu W_2(Q^2, \nu^2) &\rightarrow F_2(Q^2/\nu^2); \end{aligned} \quad (3)$$

i.e., that in inclusive, deep inelastic processes  $W_{1/2}$  are functions only of  $x := Q^2/\nu^2$  and not of  $Q^2$  and  $\nu^2$  independently.

Such experiments were first performed at SLAC in the late sixties and have been extended widely since then. Equation (3) is confirmed completely,<sup>1</sup> it is correct as  $Q^2$  varies over four orders-of-magnitude. The presence of pointlike constituents is the only possible explanation of this behaviour, and many other observations made in such experiments. Hence quarks exist but are “confined” in colourless bound states, and understanding the origin and meaning of that confinement is another focus of these notes.

The role that quarks play in hadron structure is a primary subject of contemporary experimental and theoretical nuclear physics and it is not necessary to employ high energy or large momentum transfer to explore it. The electromagnetic form factor of the neutron is a good example. The differential cross section for electron-neutron scattering:

$$\frac{d\sigma}{d\Omega} = \frac{d\sigma}{dQ^2} \Big|_{\text{Mott}} \left( \frac{G_E^2(Q^2) + \tau G_M^2(Q^2)}{1 + \tau} + 2\tau G_M^2(Q^2) \tan^2 \frac{\theta}{2} \right), \quad (4)$$

$\tau := Q^2/(4M_N^2)$ , involves the “Mott”-term, which describes electron scattering from a point source, and the electric and magnetic form factors,  $G_E$  and  $G_M$ , that describe the structure of the neutron. Of particular interest is the electric form factor. For a neutral particle  $G_E(Q^2 = 0) = 0$ , and it is identically zero for a neutral point particle. Therefore deviations from zero are a good measure of ones description of the internal structure of the neutron.

The neutron charge radius has been measured<sup>2</sup> in the transmission of low energy neutrons through Pb atoms:

$$r_n^2 := -6 \frac{dG_E(Q^2)}{dQ^2} \Big|_{Q^2=0} = -0.113 \pm 0.003 \text{ fm}^2. \quad (5)$$

It is negative and that must be understood. In studies<sup>3,4</sup> of  $K^0$  and  $K^{0*}$  mesons one finds  $r_{K^0}^2 < 0$  and  $r_{K^{0*}}^2 < 0$ . These results are understood simply: the mesons are  $\bar{s}$ - $d$  bound states and, being lighter, the negatively charged  $d$ -quark is able to propagate further from the system’s centre-of-mass thereby generating a negative charge-distribution at long-range. That mechanism generates 60% of the observed value:<sup>5</sup>  $r_{K^0}^2 = -0.054 \pm 0.026 \text{ fm}^2$ , and something similar is likely to be responsible for a large part of  $r_n^2$ .

The  $Q^2$ -evolution of the form factors is more difficult to measure. In the absence of free neutron targets it must be inferred from the scattering of electrons from loosely-bound collections of polarised nucleons; e.g., deuterium or  $^3\text{He}$ . However, even in such loosely bound systems the inferred cross section is sensitive to details of the model used to calculate the nuclear wave function and the current operator, although it is anticipated that these effects can be minimised in double polarisation experiments.<sup>6</sup> The present status of measurements of  $G_E^n$  is illustrated in Fig. 1.

Such complications often arise in prospecting for quarks and gluons. However, their role in hadron structure is identifiable only in the signatures they write in, for example, the  $Q^2$ -dependence of form factors, so the difficulties must be overcome. The accurate calculation of form factors on the entire domain of accessible  $Q^2$  can be a very good test of any given description of

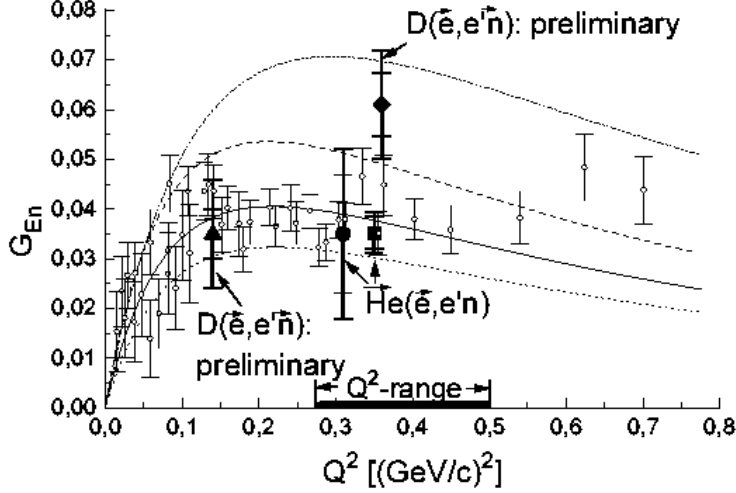


Figure 1:  $G_E^n$  - summary of data<sup>6</sup>. The lines are two-parameter fits using different  $N$ - $N$  potentials in the calculation of the deuterium wave function. The “ $Q^2$ -range” is that of a recent MAMI [Mainz] experiment:  ${}^3\text{He}(\bar{e}, e'n)$ .

hadron structure. It relies on combining an understanding of confinement and DCSB with that of the intrinsically nonperturbative analysis of bound state structure. This synthesis is the primary focus of these notes.

Given that at low-energy and small- $Q^2$  the strong interaction is characterised by the nonperturbative phenomena of confinement, DCSB and the behaviour of colourless bound states, is its study ever simple? Yes, in scattering processes at high-energy or large- $Q^2$  where perturbation theory is applicable because QCD is asymptotically free. As described in Sec. 1.2, the coupling constant evolves with  $Q^2$ :

$$\alpha_S(Q^2) \xrightarrow{Q^2 \rightarrow \infty} 0, \quad (6)$$

and hence quarks and gluons behave as weakly interacting, massless particles when the momentum transfer is large.

This also leads to the identification of another nonperturbative phenomenon. If one introduces the intensive variables: temperature,  $T$ , and quark chemical potential,  $\mu$ , QCD acquires additional mass-scales with which the coupling can *run*. Hence,

$$\alpha_S(Q^2 = 0; T, \mu) \sim 0 \text{ for } T \gg \Lambda_{\text{QCD}} \text{ and/or } \mu \gg \Lambda_{\text{QCD}}, \quad (7)$$

where  $\Lambda_{\text{QCD}} \sim 200 \text{ MeV}$  is the intrinsic, renormalisation-induced mass-scale in QCD. It follows that at finite- $(T, \mu)$  there is a phase of QCD in which quarks and gluons are weakly interacting, *irrespective* of the momentum transfer;<sup>7</sup> i.e., a quark-gluon plasma [QGP]. In this phase confinement and DCSB are absent and the nature of the strong interaction spectrum is qualitatively different. Phase transitions are intrinsically nonperturbative phenomena.

### 1.1 Modern Experimental Tools

Understanding the strong interaction, applying nonperturbative methods in QCD, is a difficult problem. As in all of physics, progress here and the development of understanding is promoted by the challenge of explaining real data, and there is a new generation of experimental facilities whose goal is to furnish this challenge.

DESY<sup>8</sup> [Deutsches Elektronen-Synchrotron] in Hamburg is the site of the Hadron-Electron Ring Accelerator facility [HERA]. It is a collider: in a 6 336 m underground tunnel a longitudinally-polarised, 30 GeV  $e^-$  or  $e^+$  beam collides with a counter-circulating, 820 GeV proton beam at four interaction zones. There are currently three large experimental collaborations using HERA: H1 [since 1992], ZEUS [since 1992] and HERMES [since 1995], with the goal of elucidating the internal structure of the nucleon.

Newport News, Virginia, is the site of the Thomas Jefferson National Accelerator Facility<sup>9</sup> [TJNAF, formerly CEBAF]. This machine currently accelerates electrons to 4 GeV in five circuits of an oval-shaped, 1 400 m underground tunnel. The electrons are then focused into three large, underground target areas: Halls - A [50 m diameter], B [30 m] and C [50 m]. Although Hall B is not yet fully operational, experiments have been underway in Halls A and C for two years. Many have been completed and other important experiments are underway; e.g., Hall C is currently hosting a measurement of the electromagnetic pion form factor, which will probe the evolution from the nonperturbative to the perturbative domain in QCD, and that of  $G_E^n$  is scheduled. The facility plans to expand the research capability of the accelerator by raising the beam energy to 12 GeV by the year 2006.

Cornell University in Ithaca, New York, is the site of the Cornell Electron Storage Ring<sup>10</sup> [CESR]. A circular  $e^+e^-$  collider, 12 m underground with a circumference of 768 m, CESR is a  $b$ -quark factory. With the CESR collision energy tuned to that of the  $\Upsilon(4s)$   $b$ - $\bar{b}$ -resonance, which is massive enough to decay to a  $B\bar{B}$  meson pair, the CLEO detector is able to observe the decays of  $B$ -mesons. A careful analysis of these decays can provide tight constraints on the elements of the Cabibbo-Kobayashi-Maskawa [CKM] matrix, which

describes the mixing of the eigenstates of the strong and weak interactions. Most of what is currently known about  $B$ -meson decays is due to experiments using the CLEO detector. However, since experiments using  $B$ -mesons are a far-reaching tool to probe the standard model, it is anticipated that the next five years will see the construction of three more  $b$ -factories: at KEK in Japan; at SLAC; and in the completion of the HERA-B site at DESY. Heavy-quark physics is a burgeoning, contemporary focus.

Brookhaven National Laboratory<sup>11</sup> [BNL] is the site of the AGS [Alternating Gradient Synchrotron] and the future site of RHIC, the Relativistic Heavy Ion Collider. Its relativistic heavy ion programme currently focuses on the study of nuclear matter at extremes of temperature and density, and prospecting for the quark gluon plasma. The AGS has been operating since 1962 and its fixed target experiments are laying the foundations of the search for the QGP. In the future, the AGS will act as an injector for RHIC, which is due for completion in 1999. Using two concentric rings, each 3.8 km in diameter, RHIC will collide two 100 A GeV  $^{197}\text{Au}$  beams at several detector sites around the ring. Producing a total centre-of-mass energy of  $\sim 40$  TeV at each collision site, RHIC is expected to produce an equilibrated QGP, approaching it along a high- $T$ , baryon-poor trajectory.

Also in the hunt for the QGP is the SpS [Super-proton Synchrotron] at CERN,<sup>12</sup> seven kilometres in circumference. Fixed target experiments with S+Pb at  $\sim 200$  A GeV and Pb + Pb at  $\sim 160$  A GeV are possible using this machine, producing much higher centre-of-mass energies than those available at the AGS. With these resources, experiments CERES/NA45 and NA50 have observed interesting effects: an enhancement in the dilepton spectrum and a suppression of the  $\psi$ -production cross section. Whether these signal the formation of a QGP is an unresolved issue but their explanation is certainly providing a challenge to theory. The next phase is the construction of the LHC [Large Hadron Collider]. Currently anticipated to be completed in 2005, it will share the 27 km LEP tunnel and be capable of hosting heavy ion collisions that generate a centre-of-mass energy thirty-times greater than that possible at RHIC. If the QGP is not discovered with RHIC then the LHC can still promise to do so. If it is, then the LHC should provide a tool for thoroughly exploring its properties, and for many other things.

I have surveyed only a few of the many existing and planned experimental facilities. Nevertheless, the intensity of effort being expended in prospecting for quarks and gluons, and in elucidating the subtle properties of QCD, is obvious in this. More detailed information is available at the web sites I have indicated and obvious searches will yield details about other facilities.

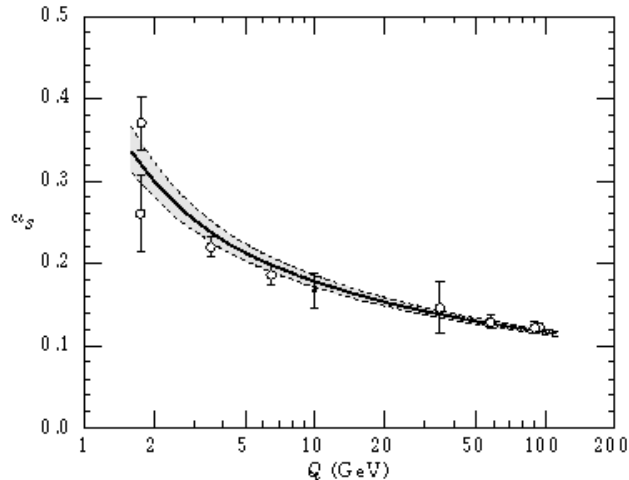


Figure 2: Summary<sup>1</sup> of the values of  $\alpha_{\text{QCD}}(Q)$  at the points where they are measured. The lines show the central values and the  $\pm\sigma$  limits of the average.

### 1.2 Perturbative QCD

QCD is a gauge theory, which in some respects is like QED. The elementary fermions, quarks in this case, interact by exchanging massless vector bosons: gluons. In QCD the coupling is through the colour quantum number: the colour charge is the analogue of the electric charge. The special feature of QCD is that the gluon carries the colour charge, as well as the quarks, and that means the gluons are self-interacting, which is enough to completely change the qualitative character of the theory.

In both QED and QCD the coupling “constant” is not constant at all but evolves with  $Q^2$  and it can be calculated perturbatively:

$$\alpha_{\text{QED}} = \frac{\alpha}{1 - \alpha/3\pi \ln(Q^2/m_e^2)}, \quad \alpha \simeq \frac{1}{137}, \quad (8)$$

$$\alpha_{\text{S}} = \frac{12\pi}{(11N_c - 2N_f) \ln(Q^2/\Lambda_{\text{QCD}}^2)}, \quad (9)$$

where the “ $11N_c$ ”,  $N_c = 3$  is the number of colours, appears because the gluons are self-interacting.  $N_f$  is the number of fermion flavours. As depicted in Fig. 2,  $\alpha_{\text{S}}(Q)$  decreases with increasing- $Q$ , which is opposite to the behaviour of  $\alpha_{\text{QED}}(Q)$  quoted in Eq. (8). The rate of the evolution is also very different, being determined by vastly different mass-scales:  $\Lambda_{\text{QCD}}/m_e \sim 450$ . The

reduction in  $\alpha_S$  with increasing  $Q$  is called “asymptotic freedom”. It is due to gluon self-interactions and entails that perturbation theory is valid at large- $Q^2$  in QCD; i.e., at short-distances, *not* at long-distances as in QED.

A very successful application of perturbative QCD is the calculation of

$$R := \frac{\sigma_{e^+e^- \rightarrow \text{hadrons}}}{\sigma_{e^+e^- \rightarrow \mu^+\mu^-}}, \quad (10)$$

which is known to order  $\alpha_S^3$ :

$$R = N_c \sum_{f=1}^{N_f} e_f^2 \left[ 1 + \frac{\alpha_S}{\pi} + 1.411 \left( \frac{\alpha_S}{\pi} \right)^2 - 12.8 \left( \frac{\alpha_S}{\pi} \right)^3 + \dots \right], \quad (11)$$

where  $e_f$  is the electric charge of a quark of flavour  $f$ .<sup>a</sup> The theoretical prediction is compared with experiment in Fig. 3. It proves that  $N_c = 3$  because the normalisation of the prediction is otherwise incorrect. The figure also highlights the current-quark mass thresholds and confirms the electric charge assignments: below the  $c$ -quark threshold  $R \approx N_c \sum_{f=1}^{N_f=3} e_f^2 = 2$ , then  $R \approx N_c \sum_{f=1}^{N_f=4} e_f^2 = 10/3$ , and above the  $b$ -quark threshold  $R \approx N_c \sum_{f=1}^{N_f=5} e_f^2 = 11/3$ .

Perturbation theory is the most widely used, systematic tool in physics and in QCD it is extremely accurate in high-energy processes. In addition to the calculation of  $R$ , there are many other applications which confirm QCD as the theory describing the strong interaction. However, there are domains and problems in QCD that perturbation theory simply cannot describe. This is very obvious in Fig. 2 where the coupling is seen to *increase* with the inter-particle separation: QCD becomes a strong coupling theory for  $Q < 2 \text{ GeV}$  [ $x > 0.1 \text{ fm}$ ]. Further, as observed in Sec. 1, confinement, DCSB, bound state structure and phase transitions are intrinsically nonperturbative phenomena. They are at the core of hadron physics and hence nonperturbative methods are essential in prospecting for quarks and gluons.

### 1.3 Nonperturbative Effects in QCD

The extraordinary effects in QCD can be explained in terms of the properties of *dressed*-quark and -gluon propagators. They describe the “in-medium” propagation characteristics of QCD’s elementary quanta, with the “medium” being the nontrivial ground state of QCD. A photon propagating through a

---

<sup>a</sup>This expression assumes that all the quarks are massless but it is also known for massive quarks. In comparing with data,  $b$ -quark mass corrections are important.



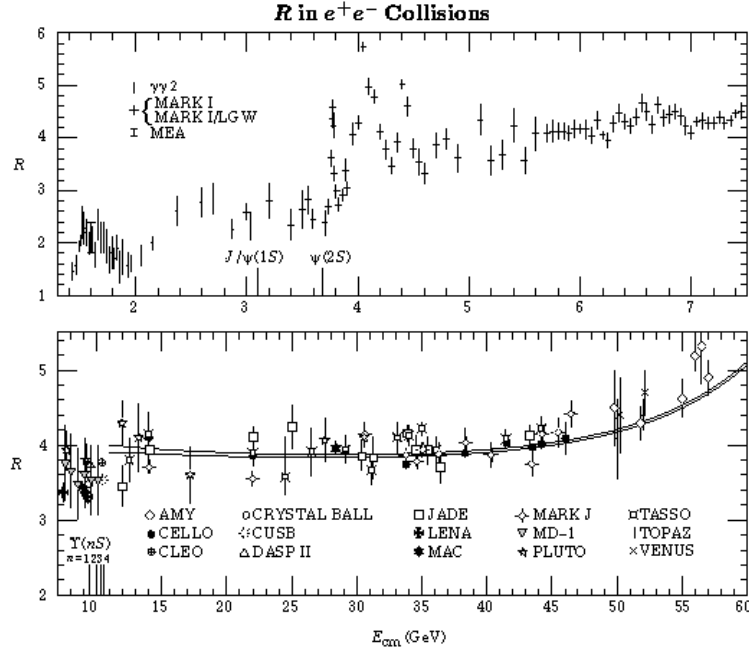


Figure 3: Selected measurements of  $R$ .<sup>1</sup> The positions of the  $\psi$ ,  $\psi(2S)$  and four lowest  $\Upsilon(nS)$  resonances are also indicated, which are not predicted by perturbation theory. A fit to the data in the lower panel yields  $\alpha_S(Q = 34 \text{ GeV}) = 0.142 \pm 0.03$ . The experimental error is larger than the theoretical uncertainty. The plotted calculations include electroweak corrections, which predict the increase as  $E_{cm} \rightarrow M_Z$ .

dense  $e^-$ -gas provides a familiar example of the effect a medium has on the propagation of an elementary particle. Due to particle-hole excitations the propagation of the photon is modified:

$$\frac{1}{Q^2} \rightarrow \frac{1}{Q^2 + m_D^2}; \quad (12)$$

i.e., the photon acquires an effective mass. The “Debye” mass,  $m_D \propto k_F$ , the Fermi momentum, and it screens the interaction so that in the dense  $e^-$ -gas the Coulomb interaction has a finite range:  $r \propto 1/m_D$ . Quark and gluon propagators are modified in a similar way. They acquire *momentum-dependent* effective masses, which have observable effects on hadron properties.

**1.3.1 Chiral symmetry.** Gauge theories with massless fermions have a chiral symmetry. Its effect can be visualised by considering the helicity:  $\lambda \propto J \cdot p$ , the

projection of the fermion's spin onto its direction of motion.  $\lambda$  is a Poincaré invariant spin observable that takes a value of  $\pm 1$ . The chirality operator can be realised as a  $4 \times 4$ -matrix,  $\gamma_5$ , and a chiral transformation is then represented as a rotation of the  $4 \times 1$ -matrix quark spinor field

$$q(x) \rightarrow e^{i\gamma_5\theta} q(x). \quad (13)$$

A chiral rotation through  $\theta = \pi/2$  has no effect on a  $\lambda = +1$  quark,  $q_{\lambda=+} \rightarrow q_{\lambda=+}$ , but changes the sign of a  $\lambda = -1$  quark field,  $q_{\lambda=-} \rightarrow -q_{\lambda=-}$ . In composite particles this is manifest as a flip in their parity:  $J^{P=+} \leftrightarrow J^{P=-}$ ; i.e., a  $\theta = \pi/2$  chiral rotation is equivalent to a parity transformation. Exact chiral symmetry therefore entails that degenerate parity multiplets must be present in the spectrum of the theory.

For many reasons, the masses of the  $u$ - and  $d$ -quarks are expected to be very small; i.e.,  $m_u \sim m_d \ll \Lambda_{\text{QCD}}$ . Therefore chiral symmetry should only be weakly broken, with the strong interaction spectrum exhibiting nearly degenerate parity partners. The experimental comparison is presented in Eq. (14):

$$\begin{array}{c|c|c} N(\frac{1}{2}^+, 938) & \pi(0^-, 140) & \rho(1^-, 770) \\ N(\frac{1}{2}^-, 1535) & a_0(0^+, 980) & a_1(1^+, 1260) \end{array}. \quad (14)$$

Clearly the expectation is very badly violated, with the splitting much too large to be described by the small current-quark masses. What is wrong?

Chiral symmetry can be related to properties of the quark propagator,  $S(p)$ . For a free quark

$$S_0(p) = \frac{m - i\gamma \cdot p}{m^2 + p^2}, \quad (15)$$

with  $\{\gamma_\mu, \mu = 1, \dots, 4\}$  the Dirac matrices, and as a matrix

$$S_0(p) \rightarrow e^{i\gamma_5\theta} S_0(p) e^{i\gamma_5\theta} = \frac{-i\gamma \cdot p}{p^2 + m^2} + e^{2i\gamma_5\theta} \frac{m}{p^2 + m^2} \quad (16)$$

under a chiral transformation. As anticipated, for  $m = 0$ ,  $S_0(p) \rightarrow S_0(p)$ ; i.e., the symmetry breaking term is proportional to the current-quark mass and it can be measured by the “quark condensate”

$$-\langle \bar{q}q \rangle := \int \frac{d^4p}{(2\pi)^4} \text{tr}[S(p)] \propto \int \frac{d^4p}{(2\pi)^4} \frac{m}{p^2 + m^2}, \quad (17)$$

which is the “Cooper-pair” density in QCD. For a free quark the condensate vanishes if  $m = 0$  but what is the effect of interactions?

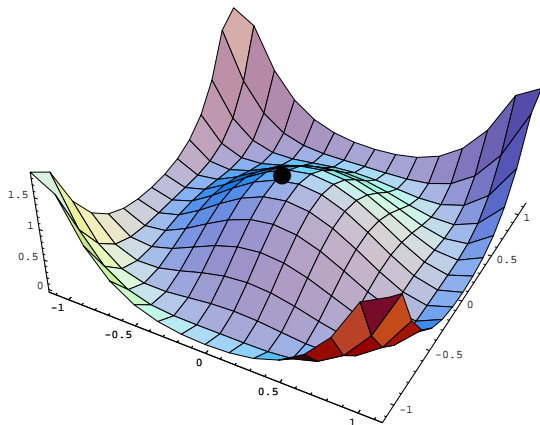


Figure 4: A rotationally invariant but unstable extremum of the Hamiltonian obtained with the potential  $V(\sigma, \pi) = (\sigma^2 + \pi^2 - 1)^2$ .

Interactions dress the quark propagator so that it takes the form

$$S(p) := \frac{1}{i\gamma \cdot p + \Sigma(p)} = \frac{-i\gamma \cdot p A(p^2) + B(p^2)}{p^2 A^2(p^2) + B^2(p^2)}, \quad (18)$$

where  $\Sigma(p)$  is the self energy, expressed in terms of the scalar functions:  $A$  and  $B$ , which are  $p^2$ -dependent because the interaction is momentum-dependent. On the valid [weak-coupling] domain they can be calculated in perturbation theory and at one-loop order

$$B(p^2) = m \left( 1 - \frac{3\alpha_S}{4\pi} \ln \left[ \frac{p^2}{m^2} \right] \right), \quad (19)$$

which is  $\propto m$ . This result persists: at every order in perturbation theory every mass-like correction to  $S(p)$  is  $\propto m$  so that  $m$  is apparently the *only* source of chiral symmetry breaking and  $\langle \bar{q}q \rangle \propto m \rightarrow 0$  as  $m \rightarrow 0$ . The current-quark masses are the only explicit chiral symmetry breaking terms in QCD.

However, symmetries can be “dynamically” broken. Consider a point-particle in a rotationally invariant potential  $V(\sigma, \pi) = (\sigma^2 + \pi^2 - 1)^2$ , where  $(\sigma, \pi)$  are the particle’s coordinates. In the state depicted in Fig. 4, the particle is stationary at an extremum of the action that is rotationally invariant but unstable. In the ground state of the system, the particle is stationary at any point  $(\sigma, \pi)$  in the trough of the potential, for which  $\sigma^2 + \pi^2 = 1$ . There are an uncountable infinity of such vacua,  $|\theta\rangle$ , which are related one to another by

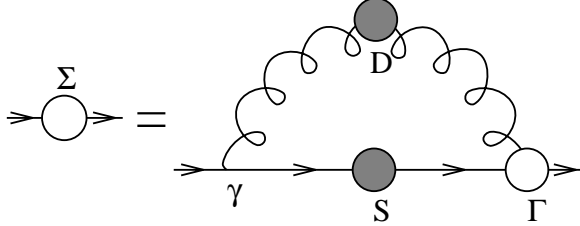


Figure 5: DSE for the dressed-quark self-energy. The kernel of this equation is constructed from the dressed-gluon propagator ( $D$  - spring) and the dressed-quark-gluon vertex ( $\Gamma$  - open circle). One of the vertices is bare (labelled by  $\gamma$ ) as required to avoid over-counting.

rotations in the  $(\sigma, \pi)$ -plane. The vacua are degenerate but not rotationally invariant and hence, in general,  $\langle \theta | \sigma | \theta \rangle \neq 0$ . In this case the rotational invariance of the Hamiltonian is not exhibited in any single ground state: the symmetry is dynamically broken with interactions being responsible for  $\langle \theta | \sigma | \theta \rangle \neq 0$ .

**1.3.2 Dynamical chiral symmetry breaking.** The analogue in QCD is  $\langle \bar{q}q \rangle \neq 0$  when  $m = 0$ . At any finite order in perturbation theory that is impossible. However, using the Dyson-Schwinger equation [DSE] for the quark self energy [the QCD “gap equation”]:

$$i\gamma \cdot p A(p^2) + B(p^2) = Z_2 i\gamma \cdot p + Z_4 m + Z_1 \int^\Lambda \frac{d^4\ell}{(2\pi)^4} g^2 D_{\mu\nu}(p-\ell) \gamma_\mu \frac{\lambda^a}{2} \frac{1}{i\gamma \cdot \ell A(\ell^2) + B(\ell^2)} \Gamma_\nu^a(\ell, p), \quad (20)$$

depicted in Fig. 5, it is possible to sum infinitely many contributions.<sup>b</sup> That allows one to expose effects in QCD which are inaccessible in perturbation theory.

The quark DSE is a nonlinear integral equation for  $A$  and  $B$  and its non-linearity is what makes it possible to generate nonperturbative effects. The kernel of the equation is composed of the dressed-gluon propagator:

$$g^2 D_{\mu\nu}(k) = \left( \delta_{\mu\nu} - \frac{k_\mu k_\nu}{k^2} \right) \frac{\mathcal{G}(k^2)}{k^2}, \quad \mathcal{G}(k^2) := \frac{g^2}{[1 + \Pi(k^2)]}, \quad (21)$$

<sup>b</sup> In Eq. (20),  $m$  is the  $\Lambda$ -dependent current-quark bare mass and  $\int^\Lambda$  represents mnemonically a *translationally-invariant* regularisation of the integral, with  $\Lambda$  the regularisation mass-scale. The final stage of any calculation is to remove the regularisation by taking the limit  $\Lambda \rightarrow \infty$ . The quark-gluon-vertex and quark wave function renormalisation constants,  $Z_1(\zeta^2, \Lambda^2)$  and  $Z_2(\zeta^2, \Lambda^2)$ , depend on the renormalisation point,  $\zeta$ , and the regularisation mass-scale, as does the mass renormalisation constant  $Z_m(\zeta^2, \Lambda^2) := Z_2(\zeta^2, \Lambda^2)^{-1} Z_4(\zeta^2, \Lambda^2)$ .

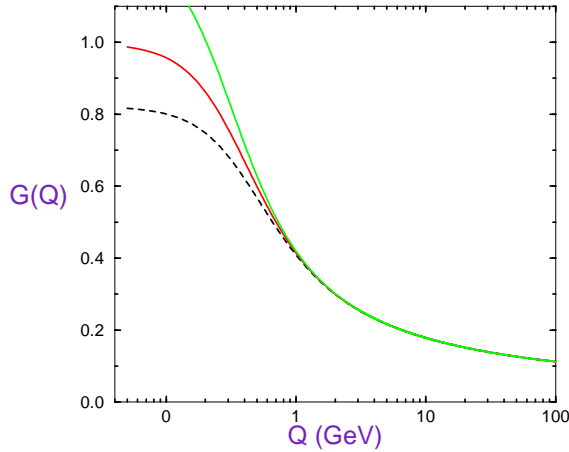


Figure 6: Illustrative forms of  $\mathcal{G}(Q)$  that agree with the perturbative result at  $Q > 1$  GeV. Three possibilities are canvassed:  $\mathcal{G}(Q = 0) < 1$ ;  $\mathcal{G}(Q = 0) = 1$ ; and  $\mathcal{G}(Q = 0) > 1$ .

where  $\Pi(k^2)$  is the vacuum polarisation, which contains all the dynamical information about gluon propagation, and the dressed-quark-gluon vertex:  $\Gamma_\mu^a(k, p)$ . The bare (undressed) vertex is

$$\Gamma_\mu^a(k, p)_{\text{bare}} = \gamma_\mu \frac{\lambda^a}{2}. \quad (22)$$

Once  $D_{\mu\nu}$  and  $\Gamma_\mu^a$  are known, Eq. (20) is straightforward to solve by iteration. One chooses an initial seed for the solution functions:  ${}_0A$  and  ${}_0B$ , and evaluates the integral on the right-hand-side (r.h.s.). The bare propagator values:  ${}_0A = 1$  and  ${}_0B = m$  are often adequate. This first iteration yields new functions:  ${}_1A$  and  ${}_1B$ , which are reintroduced on the r.h.s. to yield  ${}_2A$  and  ${}_2B$ , etc. The procedure is repeated until  ${}_nA = {}_{n+1}A$  and  ${}_nB = {}_{n+1}B$  to the desired accuracy.

It is now simple to illustrate DCSB. Using the bare vertex and  $\mathcal{G}(Q)$  depicted in Fig. 6, I solved the quark DSE in the chiral limit. If  $\mathcal{G}(Q = 0) < 1$  then  $B(p^2) \equiv 0$  is the only solution. However, when  $\mathcal{G}(Q = 0) \geq 1$  the equation admits an energetically favoured  $B(p^2) \neq 0$  solution; i.e., if the coupling is large enough then even in the absence of a current-quark mass, contrary to Eq. (19), the quark acquires a mass *dynamically* and hence

$$\langle \bar{q}q \rangle \propto \int \frac{d^4p}{(2\pi)^4} \frac{B(p^2)}{p^2 A(p^2)^2 + B(p^2)^2} \neq 0 \text{ for } m = 0. \quad (23)$$

This identifies a mechanism for DCSB in quantum field theory. The nonzero condensate provides a new, dynamically generated mass-scale and if its magnitude is large enough <sup>c</sup> it can explain the mass splitting between parity partners, and many other surprising phenomena in QCD. The simple model illustrates that DCSB is linked to the long-range behaviour of the fermion-fermion interaction and the same is true of confinement. The question is then: How does  $D_{\mu\nu}(k)$  behave in QCD?

## 2 Dyson-Schwinger Equations

In the last section I introduced the DSE for the quark self energy. It is one of an infinite tower of coupled integral equations, with the equation for a particular  $n$ -point function involving at least one  $m > n$ -point function; e.g., the quark DSE involved the dressed-gluon propagator, a 2-point function, and the dressed-quark-gluon vertex, a 3-point function. The collection of DSEs provide a Poincaré invariant, continuum approach to solving quantum field theories. However, as an infinite collection of coupled equations, a tractable problem is only obtained if one truncates the system. Historically this has provided an impediment to the application of DSEs: *a priori* it can be difficult to judge whether a particular truncation scheme will yield qualitatively or quantitatively reliable results for the quantity sought. As we saw, the DSEs are integral equations and hence the analysis of observables is a numerical problem. Therefore a critical evaluation of truncation schemes often requires access to high-speed computers.<sup>d</sup> With such tools now commonplace, this evaluation can be pursued fruitfully.

The development of efficacious truncation schemes is not a purely numerical task, and neither is it always obviously systematic. For some, this last point diminishes the appeal of the approach. However, with growing community involvement and interest, the qualitatively robust results and intuitive understanding that the DSEs can provide is becoming clear. Indeed, those familiar with the application of DSEs in the late-70s and early-80s might be surprised with the progress that has been made. It is now clear<sup>13,14</sup> that truncations which preserve the global symmetries of a theory; e.g., chiral symmetry in QCD, are relatively easy to define and implement and, while it is more difficult to preserve local gauge symmetries, much progress has been made with Abelian theories<sup>15</sup> and more is being learnt about non-Abelian ones.

The simplest truncation scheme for the DSEs is the weak-coupling expan-

---

<sup>c</sup>— $\langle\bar{q}q\rangle^{1/3}$  need only be one order-of-magnitude larger than  $m_u \sim m_d$ .

<sup>d</sup>The human and computational resources required are still modest compared with those consumed in contemporary numerical simulations of lattice-QCD.

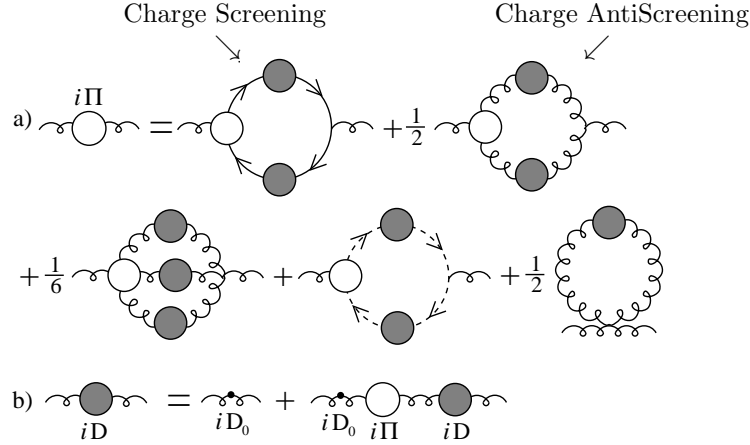


Figure 7: DSE for the gluon vacuum polarisation and propagator: solid line - quark; spring - gluon; dotted-line - ghost. The open circles are irreducible vertices. As indicated, the quark loop acts to screen the charge, as in QED, while the gluon loop opposes this, anti-screening the charge and enhancing the interaction.

sion, which shows that they *contain* perturbation theory; i.e, for any given theory the weak-coupling expansion generates all the diagrams of perturbation theory. However, as with DCSB, the most important feature of the DSEs is the antithesis of this weak-coupling expansion: the DSEs are intrinsically nonperturbative and their solution contains information that is *not* present in perturbation theory. They are ideal for studying the phenomena I identified as the core of these lectures and in this application they provide a means of elucidating identifiable signatures of the quark-gluon substructure of hadrons.

### 2.1 Gluon Propagator

In Landau gauge the dressed-gluon propagator has the form in Eq. (21) and satisfies the DSE [a nonlinear integral equation] depicted in Fig. 7. A weak coupling expansion of the equation reproduces perturbation theory and shows directly that in the one-loop expression for the running coupling constant, Eq. (9), the “ $11N_c$ ” comes from the charge-antiscreening gluon loop and the “ $2N_f$ ” from the charge-screening fermion loop. This illustrates how the non-Abelian structure of QCD is responsible for asymptotic freedom and suggests that confinement is related to the importance of gluon self-interactions.

Studies of the gluon DSE have been reported by many authors<sup>16</sup> with the conclusion that if the ghost-loop is unimportant, then the charge-antiscreening

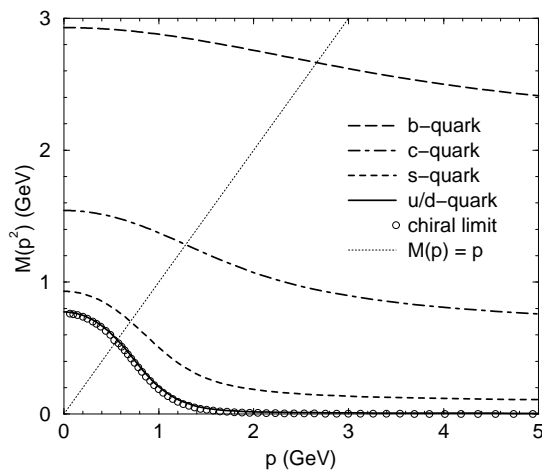


Figure 8: Dressed-quark mass-function obtained in solving the quark DSE.

3-gluon vertex dominates and, relative to the free gauge boson propagator, the dressed gluon propagator is significantly enhanced in the vicinity of  $k^2 = 0$ . The enhancement persists to  $k^2 \sim 1\text{-}2 \text{ GeV}^2$ , where a perturbative analysis becomes quantitatively reliable. In the neighbourhood of  $k^2 = 0$  the enhancement can be represented<sup>17</sup> as a regularisation of  $1/k^4$  as a distribution. A dressed-gluon propagator of this type generates confinement and DCSB *without* fine-tuning, as I will elucidate.

## 2.2 Quark Propagator

In a covariant gauge the dressed-quark propagator can be written in a number of equivalent forms: those in Eq. (18) and also as

$$S(p) = -i\gamma \cdot p \sigma_V(p^2) + \sigma_S(p^2) = \frac{Z(p^2)}{i\gamma \cdot p + M(p^2)}. \quad (24)$$

As depicted in Fig. 8, solving the quark DSE, Eq. (20), using a dressed-gluon propagator of the type described above, one obtains a quark mass-function,  $M(p^2)$ , that mirrors the enhancement of the dressed-gluon propagator. The results in the figure were obtained<sup>18</sup> with current-quark masses corresponding



to

$$\begin{array}{cccc} m_{u/d}^{1\text{ GeV}} & m_s^{1\text{ GeV}} & m_c^{1\text{ GeV}} & m_b^{1\text{ GeV}} \\ 6.6\text{ MeV} & 140\text{ MeV} & 1.0\text{ GeV} & 3.4\text{ GeV} . \end{array} \quad (25)$$

The quark DSE was also solved in the chiral limit, which in QCD is obtained by setting the Lagrangian current-quark bare mass to zero.<sup>18</sup> One observes immediately that the mass-function is nonzero even in this case. That *is* DCSB: a momentum-dependent quark mass, generated dynamically, in the absence of any term in the action that breaks chiral symmetry explicitly. This entails a nonzero value for the quark condensate in the chiral limit. That  $M(p^2) \neq 0$  in the chiral limit is independent of the details of the infrared enhancement in the dressed-gluon propagator.

Figure 8 illustrates that for light quarks ( $u$ ,  $d$  and  $s$ ) there are two distinct domains: perturbative and nonperturbative. In the perturbative domain the magnitude of  $M(p^2)$  is governed by the the current-quark mass. For  $p^2 < 1\text{ GeV}^2$  the mass-function rises sharply. This is the nonperturbative domain where the magnitude of  $M(p^2)$  is determined by the DCSB mechanism; i.e., the enhancement in the dressed-gluon propagator. This emphasises that DCSB is more than just a nonzero value of the quark condensate in the chiral limit!

The solution of  $p^2 = M^2(p^2)$  defines a Euclidean constituent-quark mass,  $M^E$ . For a given quark flavour, the ratio  $\mathcal{L}_f := M_f^E/m_f^\zeta$  is a single, quantitative measure of the importance of the DCSB mechanism in modifying the quark's propagation characteristics. As illustrated in Eq. (26),

$$\begin{array}{c|c|c|c|c|c} \text{flavour} & u/d & s & c & b & t \\ \hline \frac{M^E}{m^\zeta_{\sim 20\text{ GeV}}} & 150 & 10 & 2.3 & 1.4 & \rightarrow 1 \end{array}, \quad (26)$$

this ratio provides for a natural classification of quarks as either light or heavy. For light-quarks  $\mathcal{L}_f$  is characteristically 10-100 while for heavy-quarks it is only 1-2. The values of  $\mathcal{L}_f$  signal the existence of a characteristic DCSB mass-scale:  $M_\chi$ . At  $p^2 > 0$  the propagation characteristics of a flavour with  $m_f^\zeta < M_\chi$  are altered significantly by the DCSB mechanism, while for flavours with  $m_f^\zeta \gg M_\chi$  it is irrelevant, and explicit chiral symmetry breaking dominates. It is apparent from Eq. (26) that  $M_\chi \sim 0.2\text{ GeV} \sim \Lambda_{\text{QCD}}$ . This forms a basis for many simplifications in the study of heavy-meson observables.<sup>19</sup>

### 2.3 Confinement

Confinement is the absence of quark and gluon production thresholds in colour-singlet-to-singlet  $\mathcal{S}$ -matrix amplitudes. That is ensured if the dressed-quark and -gluon propagators do not have a Lehmann representation.

To illustrate a Lehmann representation, consider the 2-point free-scalar propagator:  $\Delta(k^2) = 1/[k^2 + m^2]$ . One can write

$$\Delta(z) = \int_0^\infty d\sigma \frac{\rho(\sigma)}{z + \sigma}, \quad (27)$$

where in this case the spectral density is

$$\rho(x) := \frac{1}{2\pi i} \lim_{\epsilon \rightarrow 0} [\Delta(-x - i\epsilon) - \Delta(-x + i\epsilon)] = \delta(m^2 - x), \quad (28)$$

which is non-negative. That is a Lehmann representation: each scalar function necessary to specify the  $n$ -point function completely has a spectral decomposition with non-negative spectral densities. Only those functions whose poles or branch points lie at timelike, real- $k^2$  have a Lehmann representation.

The existence of a Lehmann representation for a dressed-particle propagator is necessary if the construction of asymptotic “in” and “out” states for the associated quanta is to proceed; i.e., it is necessary if these quanta are to propagate to a “detector”. In its absence there are no asymptotic states with the quantum numbers of the field whose propagation characteristics are described by the propagator. Structurally, the nonexistence of a Lehmann representation for the dressed-propagators of elementary fields ensures the absence of pinch singularities in loops and hence the absence of quark and gluon production thresholds.

The mechanism can be generalised and applied to coloured bound states, such as colour-antitriplet quark-quark composites (diquarks). A study<sup>13</sup> of the quark-quark scattering matrix shows that it does not have a spectral decomposition with non-negative spectral densities and hence there are no diquark bound states. The same argument that demonstrates the absence of diquarks in the spectrum of  $SU(N_c = 3)$  also proves<sup>14</sup> that in  $SU(N_c = 2)$  the “baryons”, which are necessarily diquarks in this theory, are degenerate with the mesons.

Dressed-gluon propagators with the infrared enhancement described above do not have a Lehmann representation and using forms like this in the kernel of the quark DSE yields a dressed-quark propagator that also does not have a Lehmann representation. In this sense confinement *breeds* confinement, without fine-tuning.

#### 2.4 Hadrons: Bound States

The properties of hadrons can be understood in terms of their substructure by studying covariant bound state equations: the Bethe-Salpeter equation [BSE] for mesons and the covariant Fadde’ev equation for baryons. The mesons have

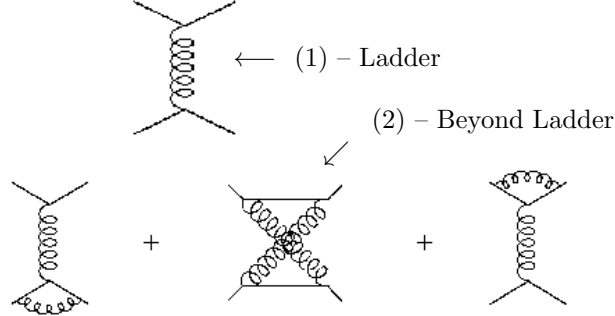


Figure 9: First two orders in a systematic expansion of the quark-antiquark scattering kernel. In this expansion, the propagators are dressed but the vertices are bare.

been studied most extensively and their internal structure is described by a Bethe-Salpeter amplitude obtained as a solution of

$$[\Gamma_H(k; P)]_{tu} = \int^\Lambda \frac{d^4 q}{(2\pi)^4} [\chi_H(q; P)]_{sr} K_{tu}^{rs}(q, k; P), \quad (29)$$

where  $\chi_H(q; P) := \mathcal{S}(q_+) \Gamma_H(q; P) \mathcal{S}(q_-)$ ;  $\mathcal{S}(q) = \text{diag}(S_u(q), S_d(q), S_s(q), \dots)$ ;  $q_+ = q + \eta_P P$ ,  $q_- = q - (1 - \eta_P) P$ , with  $P$  the total momentum of the bound state; and  $r, \dots, u$  represent colour-, Dirac- and flavour-matrix indices. The amplitude for a pseudoscalar bound state has the form

$$\begin{aligned} \Gamma_H(k; P) = T^H \gamma_5 \bigg[ & iE_H(k; P) + \gamma \cdot P F_H(k; P) \\ & + \gamma \cdot k \, k \cdot P G_H(k; P) + \sigma_{\mu\nu} k_\mu P_\nu H_H(k; P) \bigg], \end{aligned} \quad (30)$$

where  $T^H$  is a flavour matrix that determines the channel under consideration; e.g.,  $T^{K^+} := (1/2) (\lambda^4 + i\lambda^5)$ , with  $\{\lambda^j, j = 1 \dots 8\}$  the Gell-Mann matrices.

In Eq. (29),  $K$  is the renormalised, fully-amputated, quark-antiquark scattering kernel and important in the successful application of DSEs is that it has a systematic skeleton expansion in terms of the elementary, dressed-particle Schwinger functions; e.g., the dressed-quark and -gluon propagators. The expansion introduced in Ref. [13] provides a means of constructing a kernel that, order-by-order in the number of vertices, ensures the preservation of vector and axial-vector Ward-Takahashi identities; i.e., current conservation.

In any study of meson properties, one chooses a truncation for  $K$ . The BSE is then fully specified and straightforward to solve, yielding the bound

state mass and amplitude. The “ladder” truncation of  $K$  combined with the “rainbow” truncation of the quark DSE [ $\Gamma_\mu \rightarrow \gamma_\mu$  in Eq. (20)] is the simplest and most often used. The expansion of Fig. 9 provides the explanation<sup>13</sup> for why this Ward-Takahashi identity preserving truncation is accurate for flavour-nonsinglet pseudoscalar and vector mesons: there are cancellations between the higher-order diagrams. It also shows why it provides a poor approximation in the study of scalar mesons, where the higher-order terms do not cancel, and for flavour-singlet mesons, where it omits timelike gluon exchange diagrams.

### 3 A Bound State Mass Formula

The dressed-axial-vector vertex satisfies a DSE whose kernel is  $K$ , and because of the systematic expansion described in Sec. 2.4 it follows<sup>18</sup> that the axial-vector Ward-Takahashi identity [AV-WTI]:

$$-iP_\mu \Gamma_{5\mu}^H(k; P) = \mathcal{S}^{-1}(k_+) \gamma_5 \frac{T^H}{2} + \gamma_5 \frac{T^H}{2} \mathcal{S}^{-1}(k_-) - M_{(\zeta)} \Gamma_5^H(k; P) - \Gamma_5^H(k; P) M_{(\zeta)}, \quad (31)$$

[ $M_{(\zeta)} = \text{diag}(m_u^\zeta, m_d^\zeta, m_s^\zeta, \dots)$  is the current-quark mass matrix] is satisfied in any thoughtful truncation of the DSEs. That entails many important results.

**$f_H$ :** The axial-vector vertex has a pole at  $P^2 = -m_H^2$  whose residue is  $f_H$ , the leptonic decay constant:

$$f_H P_\mu = Z_2 \int^\Lambda \frac{d^4 q}{(2\pi)^4} \frac{1}{2} \text{tr} \left[ (T^H)^\dagger \gamma_5 \gamma_\mu \mathcal{S}(q_+) \Gamma_H(q; P) \mathcal{S}(q_-) \right], \quad (32)$$

with the trace over colour, Dirac and flavour indices. This expression is exact: the dependence of  $Z_2$  on the renormalisation point, regularisation mass-scale and gauge parameter is just that necessary to ensure that the l.h.s. is independent of all these things.

**Goldstone’s Theorem:** In the chiral limit

$$\begin{aligned} f_H E_H(k; 0) &= B_0(k^2), & F_R(k; 0) + 2 f_H F_H(k; 0) &= A_0(k^2), \\ G_R(k; 0) + 2 f_H G_H(k; 0) &= 2 A'_0(k^2), & H_R(k; 0) + 2 f_H H_H(k; 0) &= 0, \end{aligned} \quad (33)$$

where  $A_0(k^2)$  and  $B_0(k^2)$  are the solutions of Eq. (20) in the chiral limit, and  $F_R$ ,  $G_R$  and  $H_R$  are calculable functions in  $\Gamma_{5\mu}^H$ . This shows that when chiral symmetry is dynamically broken: 1) the flavour-nonsinglet, pseudoscalar BSE has a massless solution; 2) the Bethe-Salpeter amplitude for the massless bound state has a term proportional to  $\gamma_5$  alone, with the momentum-dependence of  $E_H(k; 0)$  completely determined by that of  $B_0(k^2)$ , in addition to terms

proportional to other pseudoscalar Dirac structures that are nonzero in general; and 3) the axial-vector vertex,  $\Gamma_{5\mu}^H(k; P)$ , is dominated by the pseudoscalar bound state pole for  $P^2 \simeq 0$ . The converse is also true. Hence, in the chiral limit, the pion is a massless composite of a quark and an antiquark, each of which has an effective mass  $M^E \sim 450 \text{ MeV}$ . With an infrared enhanced dressed-gluon propagator of the type described in Sec. 2.1, this occurs without fine-tuning.

**In-meson Condensate:** The pseudoscalar vertex also has a pole at  $P^2 = -m_H^2$  whose residue is

$$ir_H = Z_4 \int^\Lambda \frac{d^4 q}{(2\pi)^4} \frac{1}{2} \text{tr} \left[ (T^H)^\dagger \gamma_5 \mathcal{S}(q_+) \Gamma_H(q; P) \mathcal{S}(q_-) \right] := - \frac{\langle \bar{q}q \rangle_\zeta^H}{f_H}. \quad (34)$$

The renormalisation constant  $Z_4$  on the r.h.s. depends on the gauge parameter, the regularisation mass-scale and the renormalisation point. This dependence is exactly that required to ensure  $r_H$  is finite in the limit  $\Lambda \rightarrow \infty$  and gauge-parameter independent.  $\langle \bar{q}q \rangle_\zeta^H$  is the in-meson quark condensate.

**Mass Formula:** There is an identity between the residues of the pseudoscalar meson pole in the axial-vector and pseudoscalar vertices that is satisfied independent of the magnitude of the current-quark mass:

$$f_H^2 m_H^2 = -\mathcal{M}_H \langle \bar{q}q \rangle_\zeta^H, \quad \mathcal{M}_H := \text{tr}_{\text{flavour}} \left[ M_{(\zeta)} \left\{ T^H, (T^H)^\dagger \right\} \right], \quad (35)$$

e.g., for the  $\pi$ :  $\mathcal{M}_H = m_u^\zeta + m_d^\zeta$ . This is a mass formula for flavour-octet pseudoscalar mesons and the r.h.s. does not involve a difference of massive quark propagators: a phenomenological assumption often employed. The renormalisation point dependence of  $\langle \bar{q}q \rangle_\zeta^H$  is exactly such that the r.h.s. of Eq. (35) is renormalisation point *independent*.

### 3.1 A Corollary

For small current-quark masses, using Eqs. (30) and (33), Eq. (34) yields

$$r_H^0 = - \frac{1}{f_H^0} \langle \bar{q}q \rangle_\zeta^0, \quad - \langle \bar{q}q \rangle_\zeta^0 := Z_4(\zeta^2, \Lambda^2) N_c \int_q^\Lambda \text{tr}_{\text{Dirac}} [S_{\hat{m}=0}(q)], \quad (36)$$

where the superscript “0” denotes that the quantity is evaluated in the chiral limit and  $\langle \bar{q}q \rangle_\zeta^0$ , as defined here, is the chiral limit *vacuum quark condensate*; i.e., the in-meson condensate becomes the vacuum quark condensate in the chiral limit. One obtains immediately from Eqs. (35) and (36)

$$f_\pi^2 m_\pi^2 = - \left[ m_u^\zeta + m_d^\zeta \right] \langle \bar{q}q \rangle_\zeta^0 + \mathcal{O}(\hat{m}_q^2), \quad (37)$$

$$f_{K^+}^2 m_{K^+}^2 = - \left[ m_u^\zeta + m_s^\zeta \right] \langle \bar{q}q \rangle_\zeta^0 + \mathcal{O}(\hat{m}_q^2), \quad (38)$$

which exemplify what is commonly known as the Gell-Mann–Oakes–Renner relation. [ $\hat{m}_q$  is the renormalisation-point-independent current-quark mass.] Since Eq. (35) is valid *independent* of the current-quark mass, it is also applicable to heavy pseudoscalar mesons. A corollary valid in this sector is described in Sec. 5.

#### 4 An Exemplar

I have already made use of a model<sup>18</sup> to illustrate some of the robust results of DSE studies and I will now describe and explore that model in more detail. For the kernel of the quark DSE it employs the analogue of the lowest-order BSE kernel in Fig. 9:

$$\begin{aligned} Z_1 \int^\Lambda \frac{d^4 q}{(2\pi)^4} g^2 D_{\mu\nu}(p-q) \frac{\lambda^a}{2} \gamma_\mu S(q) \Gamma_\nu^a(q, p) \\ \rightarrow \int^\Lambda \frac{d^4 q}{(2\pi)^4} \mathcal{G}((p-q)^2) D_{\mu\nu}^{\text{free}}(p-q) \frac{\lambda^a}{2} \gamma_\mu S(q) \frac{\lambda^a}{2} \gamma_\nu. \end{aligned} \quad (39)$$

This is the “rainbow” approximation, in which the specification of the model is complete once a form is chosen for the “effective coupling”  $\mathcal{G}(k^2)$ .

The requirement of consistency with the AV-WTI motivates the *Ansatz*:

$$\mathcal{G}(Q^2) := 4\pi \alpha(Q^2), \quad (40)$$

so that the form of  $\mathcal{G}(Q^2)$  at large- $Q^2$  is fixed by that of the running coupling constant. This *Ansatz* is often described as the “Abelian approximation” because the l.h.s. equals the r.h.s. in QED. In QCD, equality between the two sides of Eq. (40) cannot be obtained easily by a selective resummation of diagrams. As reviewed in Ref. [16], Eqs. (5.1) to (5.8), it can only be achieved by enforcing equality between the renormalisation constants for the ghost-gluon vertex and ghost wave function:  $\tilde{Z}_1 = \tilde{Z}_3$ .

The explicit form of the *Ansatz* employed in Ref. [18] is depicted in Fig. 10 and its qualitative features are easily understood. In the infrared it has an integrable singularity<sup>20</sup>  $\propto \delta^4(k)$  and a finite-width approximation to  $\delta^4(k)$ , normalised such that it has the same  $\int d^4 k$  as the first term, and in the ultraviolet it is dominated by  $\alpha(k^2)/k^2$ . However, it does not have a singularity on the real- $k^2$  axis, which ensures gluon confinement through the absence of a Lehmann representation, Sec. 2.3.

The model has ostensibly three parameters:  $D$ , a mass-scale, and  $\omega$  and  $m_t$ , two range parameters. However, in the numerical studies the values  $\omega = 0.3 \text{ GeV}$  [=  $1/(\cdot 66 \text{ fm})$ ] and  $m_t = 0.5 \text{ GeV}$  [=  $1/(\cdot 39 \text{ fm})$ ] were fixed, and only  $D$

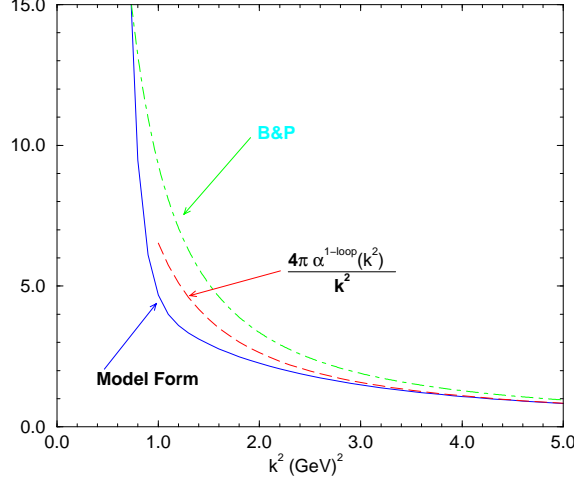


Figure 10: *Ansatz* for  $\mathcal{G}(k^2)/k^2$  employed in Ref. [18]. “B&P” labels a solution<sup>17</sup> of the gluon DSE, which is presented for comparison, as is the one-loop running coupling in QCD.

and the renormalised  $u/d$ - and  $s$ -current-quark masses varied in order to satisfy the goal of a good description of low-energy  $\pi$ - and  $K$ -meson properties. This was achieved with

$$D = 0.781 \text{ GeV}^2, \quad m_{u/d}^\zeta = 3.74 \text{ MeV}, \quad m_s^\zeta = 82.5 \text{ MeV}, \quad (41)$$

at  $\zeta \approx 20 \text{ GeV}$ , which is large enough to be in the perturbative domain.

As remarked in Sec. 1.3, the chiral limit is unambiguously defined by  $\hat{m} = 0$  so there is no perturbative contribution to the scalar piece of the quark self energy,  $B(p^2)$ ; and in fact there is no scalar, mass-like divergence in the perturbative calculation of the self energy.

Figure 11 depicts the dressed-quark mass function,  $M(p^2)$ , obtained by solving the quark DSE using the parameters in Eq. (41), and in the chiral limit. It complements Fig. 8 by highlighting the qualitative difference between the behaviour of  $M(p^2)$  in the chiral limit and in the presence of explicit chiral symmetry breaking. In the latter case

$$M(p^2) \stackrel{\text{large-}p^2}{=} \frac{\hat{m}}{\left(\frac{1}{2} \ln \left[ \frac{p^2}{\Lambda_{\text{QCD}}^2} \right] \right)^{\gamma_m}} \{1 + \text{two loop}\}, \quad \gamma_m = \frac{12}{33 - 2N_f}. \quad (42)$$

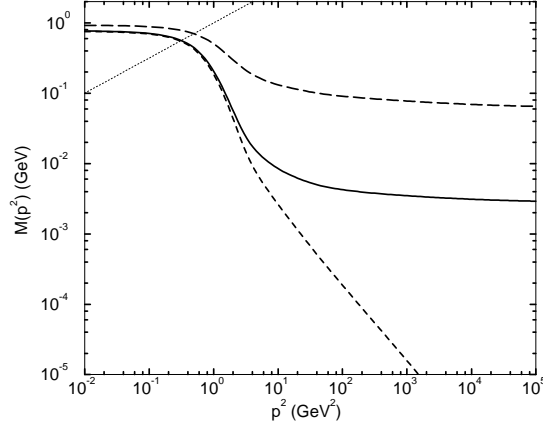


Figure 11: Dressed-quark mass function obtained in solving the quark DSE using the parameters in Eq. (41):  $u/d$ -quark (solid line);  $s$ -quark (long-dashed line); chiral limit (dashed line). The renormalisation point is  $\zeta \approx 20 \text{ GeV}$ . The intersection of the line  $M^2(p^2) = p^2$  (dotted line) with each curve defines  $M^E$ , the Euclidean constituent-quark mass.

However, in the chiral limit the ultraviolet behaviour is

$$M(p^2) \stackrel{\text{large-}p^2}{=} \frac{2\pi^2\gamma_m}{3} \frac{(-\langle\bar{q}q\rangle^0)}{p^2 \left(\frac{1}{2} \ln \left[\frac{p^2}{\Lambda_{\text{QCD}}^2}\right]\right)^{1-\gamma_m}}, \quad (43)$$

where  $\langle\bar{q}q\rangle^0$  is the renormalisation-point-independent vacuum quark condensate. Analysing the chiral limit solution yields

$$-\langle\bar{q}q\rangle^0 = (0.227 \text{ GeV})^3, \quad (44)$$

which is a reliable means of determining  $\langle\bar{q}q\rangle^0$  because corrections to Eq. (43) are suppressed by powers of  $\Lambda_{\text{QCD}}^2/\zeta^2$ .

Equation (36) defines the renormalisation-point-dependent vacuum quark condensate

$$-\langle\bar{q}q\rangle_\zeta^0 \Big|_{\zeta=19 \text{ GeV}} := \left( \lim_{\Lambda \rightarrow \infty} Z_4(\zeta, \Lambda) N_c \int_q^\Lambda \text{tr}_{\text{Dirac}} [S_{\hat{m}=0}(q)] \right) \Big|_{\zeta=19 \text{ GeV}} \quad (45)$$

and the calculated<sup>18</sup> value is  $(0.275 \text{ GeV})^3$ . In the model it is straightforward to establish explicitly that  $m^\zeta \langle\bar{q}q\rangle_\zeta^0 = \text{constant}$ , independent of  $\zeta$ , and hence

$$m^\zeta \langle\bar{q}q\rangle_\zeta^0 := \hat{m} \langle\bar{q}q\rangle^0, \quad (46)$$



which defines the renormalisation-point-independent current-quark masses unambiguously. From this and Eqs. (41), (44) and (45) one obtains

$$\hat{m}_{u/d} = 6.60 \text{ MeV}, \quad \hat{m}_s = 147 \text{ MeV}. \quad (47)$$

Using the one-loop evolution in Eq. (42) these values yield  $m_{u/d}^\zeta = 3.2 \text{ MeV}$  and  $m_s^\zeta = 72 \text{ MeV}$ , which are within  $\sim 10\%$  of the actual values in Eq. (41). This indicates that higher-loop corrections to the one-loop formulae provide contributions of  $< 10\%$  at  $p^2 = \zeta^2$ . The magnitude of the higher-loop contributions decreases with increasing  $p^2$ .

The renormalisation-point-invariant product in Eq. (46) also yields

$$-\langle \bar{q}q \rangle_\zeta^0 \big|_{\zeta=1 \text{ GeV}} := (\ln[1/\Lambda_{\text{QCD}}])^{\gamma_m} \langle \bar{q}q \rangle^0 = (0.241 \text{ GeV})^3, \quad (48)$$

which can be compared directly with the value of the quark condensate employed in contemporary phenomenological studies:<sup>21</sup>  $(0.236 \pm 0.008 \text{ GeV})^3$ . It is now straightforward to determine the accuracy of Eqs. (37) and (38). Using experimental values on the left-hand-side, one finds:

$$(92.4 \times 138.5)^2 = (113 \text{ MeV})^4 \quad \text{cf.} \quad (111)^4 = 2 \times 5.5 \times 241^3, \quad (49)$$

$$(113 \times 495)^2 = (237 \text{ MeV})^4 \quad \text{cf.} \quad (206)^4 = (5.5 + 130) \times 241^3. \quad (50)$$

Hence, while it is good for the  $\pi$ , using the vacuum quark condensate for the kaon leads one to overestimate  $m_s^{1 \text{ GeV}}$  by 70%!

#### 4.1 Bethe-Salpeter Equation

The explicit form of the Bethe-Salpeter equation consistent with Eq. (39) is

$$0 = \Gamma_H(k; P) + \int^\Lambda \frac{d^4 q}{(2\pi)^4} \mathcal{G}((k-q)^2) D_{\mu\nu}^{\text{free}}(k-q) \frac{\lambda^a}{2} \gamma_\mu \mathcal{S}(q_+) \Gamma_H(q; P) \mathcal{S}(q_-) \frac{\lambda^a}{2} \gamma_\nu = 0. \quad (51)$$

With the *Ansatz* for  $\mathcal{G}(k^2)$  and the solution of the quark DSE for  $S(p)$ , the kernel of the BSE is specified completely. It is a linear integral equation and solving to obtain  $\Gamma_H(k; P)$  and the bound state mass is a straightforward numerical problem. Having  $D_{\mu\nu}(k)$ ,  $S(p)$  and  $\Gamma_H(k; P)$ , the calculation of observables such as: the leptonic decay constant; meson charge radius,  $\langle \bar{q}q \rangle^H$ ; and electromagnetic form factor,  $F_H(Q^2)$ ; etc., is possible.

Using this exemplar one obtains, in MeV,

$$\begin{array}{cccccccc} m_\pi & f_\pi & f^0 & m_{s\bar{s}} & f_{s\bar{s}} & m_K^{\eta_P=1/2} & f_K^{\eta_P=1/2} & m_K^{\eta_P=0} & f_K^{\eta_P=0} \\ 138.5 & 92.4 & 89.8 & 685 & 129 & 497 & 109 & 497 & 109 \end{array}. \quad (52)$$

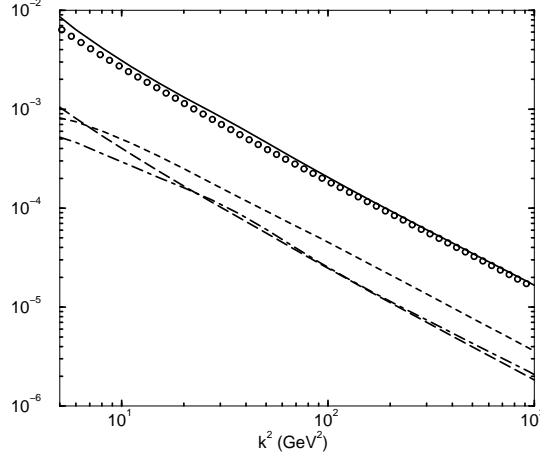


Figure 12: Asymptotic behaviour of the 0th Chebyshev moments of the functions in the  $\pi$ -meson Bethe-Salpeter amplitude:  $f_\pi {}^0E_\pi(k^2)$  (GeV, solid line);  $f_\pi {}^0F_\pi(k^2)$  (dimensionless, long-dashed line);  $k^2 f_\pi {}^0G_\pi(k^2)$  (dimensionless, dashed line); and  $k^2 f_\pi {}^0H_\pi(k^2)$  (GeV, dot-dashed line). The  $k^2$ -dependence is identical to that of the chiral-limit quark mass function,  $M(p^2)$ , Eq. (43). For other pseudoscalar mesons the momentum dependence of these functions is qualitatively the same, although the normalising magnitude differs.

$f^0$  is the leptonic decay constant of a pseudoscalar meson in the chiral limit and “ $s\bar{s}$ ” denotes a fictitious pseudoscalar bound state. As emphasised by Eq. (52), observables are independent of the momentum partitioning parameter,  $\eta_P$ , when all the amplitudes in Eq. (30) are retained in solving the BSE.

One aspect of the Bethe-Salpeter amplitudes, which is particularly important in the calculation of electromagnetic form factors, is their behaviour at large- $k^2$ . It is depicted in Fig. 12, where the zeroth Chebyshev moments are

$${}^0E_H(k^2) := \frac{2}{\pi} \int_0^\pi d\beta \sin^2 \beta U_0(\cos \beta) E_H(k^2, k \cdot P; P^2), \quad (53)$$

$k \cdot P := \cos \beta \sqrt{k^2 P^2}$ , and similarly for the other functions. The momentum dependence of  ${}^0E_\pi(k^2)$  at large- $k^2$  is identical to that of the chiral-limit quark mass function,  $M(p^2)$  in Eq. (43) and characterises the form of the quark-quark interaction in the ultraviolet. Very importantly, the same is true of  ${}^0F_\pi(k^2)$ ,  $k^2 {}^0G_\pi(k^2)$  and  $k^2 {}^0H_\pi(k^2)$ , with analogous results for other mesons. This is critical, e.g., because it entails<sup>22</sup> that

$$F_\pi(q^2) \propto \frac{\alpha_S(q^2)}{q^2} \frac{(-\langle \bar{q}q \rangle_{q^2}^0)^2}{f_\pi^4}; \quad (54)$$

i.e.,  $q^2 F_\pi(q^2) \approx \text{const.}$ , up to calculable  $\ln q^2$ -corrections. If one erroneously neglects  $F$  and  $G$  in  $\Gamma_\pi$ , then<sup>23</sup>  $q^4 F_\pi(q^2) \approx \text{const.}$

## 5 Heavy Quarks

The CKM matrix characterises the difference between the mass eigenstates ( $q$ ) and weak eigenstates ( $q'$ ) in the Standard Model:

$$\begin{pmatrix} d' \\ s' \\ b' \end{pmatrix} = \begin{pmatrix} V_{ud} & V_{us} & V_{ub} \\ V_{cd} & V_{cs} & V_{cb} \\ V_{td} & V_{ts} & V_{tb} \end{pmatrix} \begin{pmatrix} d \\ s \\ b \end{pmatrix}, \quad (55)$$

and the Standard Model requires that the CKM matrix be unitary. The matrix elements  $V_{qQ}$  are measurable in the semileptonic decay of a pseudoscalar meson:

$$A(P_{H_1} \rightarrow P_{H_2} \ell \nu) = \frac{G_F}{\sqrt{2}} V_{qQ} \bar{\ell} \gamma_\mu (1 - \gamma_5) \nu M_\mu^{P_{H_1} P_{H_2}}(p_1, p_2), \quad (56)$$

where  $G_F$  is the Fermi weak-decay constant and the hadronic current is

$$M_\mu^{P_{H_1} P_{H_2}}(p_1, p_2) := \langle P_{H_2}(p_2) | \bar{q} \gamma_\mu Q | P_{H_1}(p_1) \rangle \quad (57)$$

$$= f_+(t) (p_1 + p_2)_\mu + f_-(t) q_\mu, \quad (58)$$

with  $t := -q^2$ . Hence accurate measurements and calculations of these decays can decide whether or not the Standard Model is complete.

All the information about strong interaction effects in these processes is contained in the form factors,  $f_\pm(t)$ , appearing in the hadronic current, and their accurate estimation is essential to the extraction of  $V_{qQ}$  from a measurement of a semileptonic decay rate:

$$\Gamma(P_{H_1} \rightarrow P_{H_2} \ell \nu) = \frac{G_F^2}{192\pi^3} |V_{qQ}|^2 \frac{1}{m_{H_1}^3} \int_0^{t_-} dt |f_+(t)|^2 [(t_+ - t)(t_- - t)]^{3/2}, \quad (59)$$

with  $t_\pm := (m_{H_1} \pm m_{H_2})^2$  and neglecting the lepton mass. As with all form factors, the calculation of  $f_\pm(t)$  requires a knowledge of the propagation characteristics of the mesons' constituents and the structure of the bound state. The DSEs are therefore ideally suited to this analysis.

In Sec. 2.2 I introduced  $\mathcal{L}_f$ , which measures whether a quark is light or heavy. If a quark is heavy then many simplifications ensue in the calculation of hadronic observables, and they can all be traced to being able to ignore the

momentum dependence of that quark's self energy. The  $b$ -quark is certainly heavy but one cannot be as certain about the  $c$ -quark because its mass function exhibits significantly more momentum-dependence. Whether the  $c$ -quark is heavy is a qualitatively important quantitative question. It can be addressed by exploring the consequences of assuming

$$S_b(p) = \frac{1}{i\gamma \cdot p + \hat{M}_b}, \quad S_c(p) = \frac{1}{i\gamma \cdot p + \hat{M}_c}, \quad (60)$$

where  $\hat{M}_f \sim M_f^E$ . I will call this the “heavy-quark” limit.

In this limit, when the other constituent is light, it is natural to work with  $\eta_P = 1$  in Eq. (29) since the total momentum of the bound state is dominated by the momentum of the heavy-quark. Introducing the heavy-meson velocity ( $v_\mu$ ) and binding energy ( $E$ ) via

$$P := m_H v_\mu, \quad v^2 = -1; \quad M_H := \hat{M}_Q + E, \quad (61)$$

with  $M_H$  the heavy-meson mass, one finds<sup>19</sup> at leading order in  $1/M_H$

$$S(q + P) = \frac{1}{2} \frac{1 - i\gamma \cdot v}{q \cdot v - E}, \quad (62)$$

$$\Gamma_H(q; P) = \sqrt{M_H} \hat{\Gamma}_H(q; P), \quad (63)$$

where the canonical normalisation condition for  $\hat{\Gamma}_H(q; P)$  is independent of  $M_H$ . Using Eqs. (62) and (63) in Eq. (32) one obtains

$$f_H \propto 1/\sqrt{M_H}. \quad (64)$$

This is obviously not correct for light quarks since  $f_\pi < f_K$ , and the experimental situation is depicted in Fig. 13. It is clear from the figure that for the  $c$ -quark at least the  $1/\hat{M}_Q$ -corrections to Eq. (64) are significant.

The mass formula of Sec. 3 has another corollary in the heavy-quark limit: using Eq. (64) with Eqs. (34) and (35) yields

$$M_H \propto \hat{m}_Q. \quad (65)$$

A model study<sup>24</sup> shows this to be valid for  $\hat{m}_Q \gtrsim \hat{m}_s$ , which is confirmed by data, Fig. 14. Although unsurprising when one considers that  $\mathcal{O}(\hat{m}_q^2)$ -corrections to Eq. (38) are large, as noted after Eq. (50), I observe that Eq. (64) is not valid until at least  $\hat{m}_Q \gtrsim \hat{m}_c$ . Equation (65) is then only valid because of cancellations between the  $1/\hat{M}_Q$ -corrections to  $f_H$  and  $\langle \bar{q}q \rangle_\zeta^H$ .

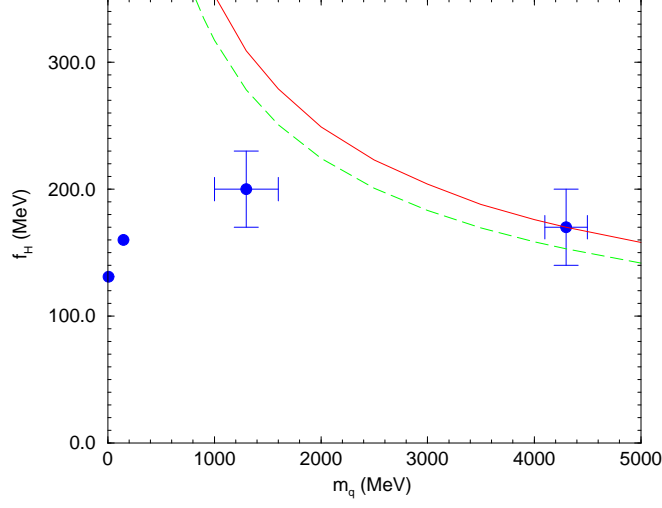


Figure 13:  $f_H$  as a function of the mass of the heaviest constituent,  $\hat{m}_q$ .<sup>1</sup> (I have included an extra, multiplicative factor of  $\sqrt{2}$ , so that  $f_\pi = 131$  MeV, which is conventional in this application.) The solid line is  $f_H(\hat{m}_q) = \text{const.}/\sqrt{\hat{m}_q}$ , fitted to  $f_B$ , while the dashed line assumes a 10% shift in  $f_B$  from  $1/\hat{m}_q$ -corrections.

### 5.1 Semileptonic Heavy $\rightarrow$ Heavy Decays

In impulse approximation the hadronic current describing  $B_f \rightarrow D_f$  decays is

$$M_\mu^{P_{H_1} P_{H_2}}(p_1, p_2) = \frac{N_c}{16\pi^4} \int d^4k \quad (66)$$

$$\text{tr} \left[ \bar{\Gamma}_{H_2}(k; -p_2) S_q(k + p_2) i\mathcal{V}_\mu^{qQ}(k + p_2, k + p_1) S_Q(k + p_1) \Gamma_{H_1}(k; p_1) S_{q'}(k) \right],$$

where  $\bar{\Gamma}_{H_2}(k; -p_2)^t := C^\dagger \Gamma_{H_2}(-k; -p_2) C$ ,  $C = \gamma_2 \gamma_4$ ,  $M^t$  is the matrix transpose of  $M$ ; and  $\mathcal{V}_\mu^{qQ}(k_1, k_2)$  is the vector part of the dressed-quark-W-boson vertex. Using Eqs. (62) and (63), and the approximation  $\mathcal{V}_\mu^{qQ}(k_1, k_2) = \gamma_\mu$ , which is valid in the heavy-quark limit,

$$f_\pm(t) = \frac{1}{2} \frac{m_{D_f} \pm m_{B_f}}{\sqrt{m_{D_f} m_{B_f}}} \xi_f(w); \quad (67)$$

i.e., the form factors are determined by a *single, universal* function:  $\xi_f(w)$ .<sup>25</sup>

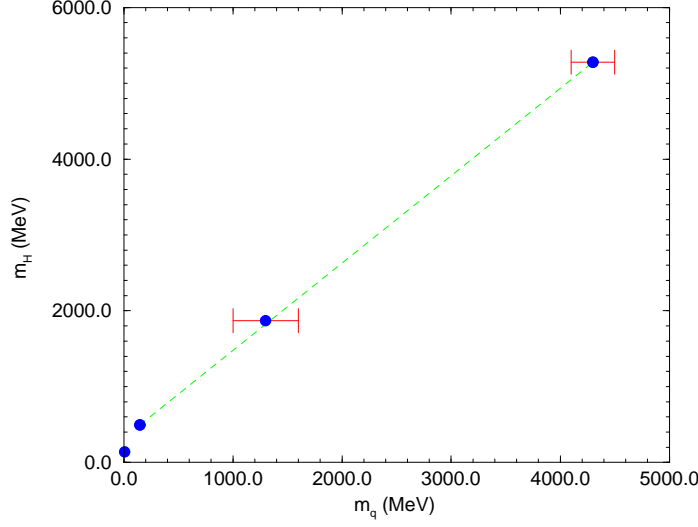


Figure 14: Pseudoscalar meson mass as a function of the mass of the heaviest constituent,  $\hat{m}_q$ .<sup>1</sup> Only the  $\pi$  does not lie on the same straight line. Since  $\hat{m}_s \lesssim M_\chi$ , the mass-scale associated with DCSB, it is not too surprising that Eq. (65) is valid for  $\hat{m}_Q \gtrsim \hat{m}_s$ : that is the domain on which explicit chiral symmetry breaking overwhelms DCSB.

Employing an *Ansatz*<sup>e</sup> for the heavy-meson Bethe-Salpeter amplitude

$$\hat{\Gamma}_{H_{1f}}(k; p_1) = \gamma_5 \left( 1 + \frac{1}{2} i \gamma \cdot v \right) \frac{1}{\kappa_f} \varphi(k^2), \quad (68)$$

where  $\kappa_f$  is the fixed, canonical Bethe-Salpeter normalisation constant for  $\hat{\Gamma}_{H_{1f}}$  and  $\phi(k^2)$  is any simple function that represents the heavy-meson as a finite-size, composite object; e.g.,

$$\phi(k^2) = \exp(-k^2/\Lambda^2), \quad (69)$$

with  $\Lambda$  a free fitting parameter, one obtains

$$\xi_f(w) = \kappa_f^2 \frac{N_c}{32\pi^2} \int_0^1 d\tau \frac{1}{W} \int_0^\infty du \varphi(z_W)^2 \left[ \sigma_S^f(z_W) + \sqrt{\frac{u}{W}} \sigma_V^f(z_W) \right], \quad (70)$$

<sup>e</sup> Ladder-like truncations of the BSE are inadequate when the mass of one or both constituents becomes large; e.g., this truncation does not yield the Dirac equation when one constituent becomes infinitely massive. Pending improved BSE studies, an *Ansatz* is used.

with  $\sigma_{S/V}^f$  the functions describing the propagation of the light-quark constituent,  $W = 1 + 2\tau(1 - \tau)(w - 1)$ ,  $z_W = u - 2E\sqrt{u/W}$  and <sup>f</sup>

$$w = \frac{m_{B_f}^2 + m_{D_f}^2 - t}{2m_{B_f}m_{D_f}} = -v_{B_f} \cdot v_{D_f} . \quad (71)$$

The normalisation of the Bethe-Salpeter amplitude ensures automatically that

$$\xi_f(w = 1) = 1 . \quad (72)$$

Experimentally measured violations of Eqs. (67) and (72) gauge the fidelity of the heavy-quark limit for physical processes.

## 5.2 Semileptonic Heavy $\rightarrow$ Light Decays

The heavy-quark limit is not really helpful in studying the decays  $B \rightarrow \pi$ ,  $D \rightarrow K$  and  $D \rightarrow \pi$  because there are only light-quarks in the final state and hence no useful expansion parameter. Therefore a theoretical description of these decays relies heavily on a good understanding of light quark propagation characteristics and the internal structure of light mesons. In this case, using Eqs. (62) and (63), the impulse approximation to the hadronic current yields<sup>19</sup>

$$f_+^{H_1 H_2}(t) = \kappa_{q'} \frac{\sqrt{2}}{f_{H_2}} \frac{N_c}{32\pi^2} F_{q'}(t; E, m_{H_1}, m_{H_2}) , \quad (73)$$

where

$$F_{q'}(t; E, m_{H_1}, m_{H_2}) = \quad (74)$$

$$\frac{4}{\pi} \int_{-1}^1 \frac{d\gamma}{\sqrt{1 - \gamma^2}} \int_0^1 d\nu \int_0^\infty u^2 du \varphi(z_1) \mathcal{E}(z_1) W_{q'}(\gamma, \nu, u) ,$$

with  $\mathcal{E}$  the pseudoscalar part of the light-meson Bethe-Salpeter amplitude and

$$W_{q'}(\gamma, \nu, u) = 2\tau^2 \left[ \sigma_S^u(z_1) \frac{d}{dz_2} \sigma_V^{q'}(z_2) - \sigma_V^u(z_1) \frac{d}{dz_2} \sigma_S^{q'}(z_2) \right] + \quad (75)$$

$$\left( 1 - \frac{u\nu}{m_{H_1}} \right) \sigma_S^u(z_1) \sigma_V^{q'}(z_2) +$$

---

<sup>f</sup>The minimum physical value of  $w$  is  $w_{\min} = 1$ , which corresponds to maximum momentum transfer with the final state meson at rest; the maximum value is  $w_{\max} \simeq (m_{B_f}^2 + m_{D_f}^2)/(2m_{B_f}m_{D_f}) = 1.6$ , which corresponds to maximum recoil of the final state meson with the charged lepton at rest.

$$\frac{1}{m_{H_1}} \left[ \sigma_S^u(z_1) \sigma_S^{q'}(z_2) + u \nu \sigma_V^u(z_1) \sigma_S^{q'}(z_2) + \right. \\ \left. (z_1 + u \nu M_{H_1}) \sigma_V^u(z_1) \sigma_V^{q'}(z_2) - 2m_{H_2}^2 \tau^2 \sigma_V^u(z_1) \frac{d}{dz_2} \sigma_V^{q'}(z_2) \right],$$

where  $\sigma'(x) := \frac{d}{dx} \sigma(x)$  and

$$z_1 = u^2 - 2u \nu E, \quad (76)$$

$$z_2 = u^2 - 2u \nu (E - X) - m_{H_2}^2 + 2i m_{H_2} \gamma u \sqrt{1 - \nu^2}, \quad (77)$$

$$X = (m_{H_1}/2) [1 + (m_{H_2}^2 - t)/m_{H_1}^2], \quad (78)$$

$$\tau = u \sqrt{1 - \nu^2} \sqrt{1 - \gamma^2}. \quad (79)$$

Under the assumption of isospin symmetry  $\sigma^u$  also represents a  $d$ -quark and, to illustrate Eq. (73), the  $B^0 \rightarrow \pi^- \ell^+ \nu_\ell$  decay is described by

$$f_+^{B\pi}(t) = \kappa_d \frac{\sqrt{2}}{f_\pi} \frac{N_c}{32\pi^2} F_d(t; E, m_B, m_\pi). \quad (80)$$

### 5.3 Calculated Transition Form Factors

With the dressed-light-quark propagators and light-meson Bethe-Salpeter amplitudes fixed completely in studies<sup>3</sup> of  $\pi$ - and  $K$ -meson properties the calculation of the heavy-meson transition form factors is straightforward. There are two free parameters: the binding energy,  $E$ , introduced in Eq. (61) and the width,  $\Lambda$ , of the heavy meson Bethe-Salpeter amplitude, introduced in Eq. (69). They were fixed<sup>19</sup> at

$$E = 0.44 \text{ GeV}, \quad \Lambda = 1.4 \text{ GeV} = 1/[0.14 \text{ fm}] \quad (81)$$

by requiring a best, weighted least-squares fit to the three available lattice data points<sup>26</sup> for  $f_+^{B\pi}$  and the experimental value<sup>27</sup> for the  $B^0 \rightarrow \pi^- \ell^+ \nu$  branching ratio. In doing that the study used  $m_B = 5.27 \text{ GeV}$  and was constrained to yield  $f_B = 0.17 \text{ GeV}$ , which is the central value favoured in a recent analysis of lattice simulations.<sup>28</sup> This procedure assumes only that the  $b$ -quark is in the heavy-quark domain and yields  $f_{B_s} = 0.18 \text{ GeV}$ .

The calculated form of  $f_+^{B\pi}(t)$  is presented in Fig. 15. A good *interpolation* of the result is provided by

$$f_+^{B\pi}(t) = \frac{0.458}{1 - t/m_{\text{mon}}^2}, \quad m_{\text{mon}} = 5.67 \text{ GeV}. \quad (82)$$



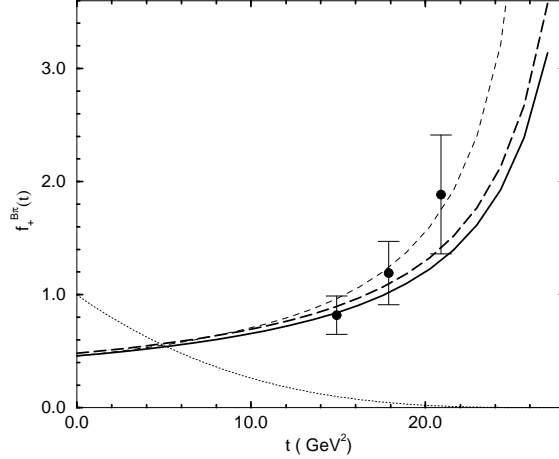


Figure 15: Calculated form of  $f_+^{B\pi}(t)$ . The solid line was obtained<sup>19</sup> assuming only that the  $b$ -quark is heavy, the dashed line assumed the same of the  $c$ -quark. The data are the results of a lattice simulation<sup>26</sup> and the light, short-dashed line is a vector dominance, monopole model:  $f_+(t) = 0.46/(1 - t/m_{B^*}^2)$ ,  $m_{B^*} = 5.325$  GeV. The light, dotted line is the phase space factor  $|f_+^{B\pi}(0)|^2 [(t_+ - t)(t_- - t)]^{3/2} / (\pi m_B)^3$  in Eq. (59), which illustrates that the  $B \rightarrow \pi e \nu$  branching ratio is determined primarily by the small- $t$  behaviour  $f_+^{B\pi}(t)$ . The calculated branching ratio is  $2.0 \times 10^{-4}$ , cf. the experimental value<sup>27</sup>  $[1.8 \pm 0.4] \times 10^{-4}$ .

This value of  $m_{\text{mon}}$  can be compared with that obtained in a fit to lattice data:<sup>26</sup>  $m_{\text{mon}} = 5.6 \pm 0.3$ . The calculated value of  $f_+^{B\pi}(0) = 0.46$  is compared with its value obtained using a range of other theoretical tools in Table 1. The uncertainty in  $f_+^{B\pi}(0)$  is the major source of the large uncertainty in the CKM matrix element:  $V_{bu} = 0.0032 \pm 0.0012$ .

The calculated form of  $\xi(w)$ , which characterises the semileptonic heavy  $\rightarrow$  heavy-meson decays, is depicted in Fig. 16. It yields a value for  $\rho^2 := -\xi'(w=1) = 0.87 - 0.92$ , close to that obtained with a linear fitting form,<sup>38</sup> however,  $\xi(w)$  has significant curvature and deviates quickly from that fit. The curvature is, in fact, very well matched to that of the nonlinear fit,<sup>38</sup> however, the value of  $\rho^2$  reported in that case is very different from the calculated value. The derivation of the formula for  $\xi(w)$  assumes that the heavy-quark limit is valid not only for the  $b$ -quark but also for the  $c$ -quark. These results therefore suggest that the latter assumption is only accurate to approximately 20%.

The calculated form of  $f_+^{DK}(t)$  is depicted in Fig. 17. The  $t$ -dependence is well-approximated by a monopole fit. The calculated value of  $f_+^{DK}(0) = 0.62$  is approximately 15% less than the experimental value.<sup>1</sup> That is also a gauge of

Reference	$f_+^{B\pi}(0)$
Ref. [19]	0.46
Dispersion relations <sup>29</sup>	$0.18 \rightarrow 0.49$
Quark Model <sup>30</sup>	$0.33 \pm 0.06$
Quark Model <sup>31</sup>	$0.21 \pm 0.02$
Quark Model <sup>32</sup>	0.29
Light-Cone Sum Rules <sup>33</sup>	$\begin{cases} 0.29 \text{ direct} \\ 0.44 \text{ pole dominance} \end{cases}$
Quark Confinement Model <sup>34</sup>	0.6
Quark Confinement Model <sup>35,36</sup>	0.53

Table 1: Comparison of the calculated result for  $f_+^{B\pi}(0)$  with a values obtained using other theoretical tools. More extensive and complementary lists are presented elsewhere.<sup>29,32,36</sup>

the size of  $1/\hat{M}_c$ -corrections, which are expected to reduce the value of the  $D$ - and  $D_s$ -meson leptonic decay constants calculated in the heavy-quark limit:  $f_D = 285 \text{ MeV}$ ,  $f_{D_s} = 298 \text{ MeV}$ . A 15% reduction yields  $f_D = 0.24 \text{ GeV}$  and  $f_{D_s} = 0.26 \text{ GeV}$ , values which are consistent with lattice estimates,<sup>28</sup> the latter with experiment,<sup>39</sup> and both with the scaling law illustrated in Fig. 13.

On the kinematically accessible domain,  $0 < t < (m_D - m_\pi)^2$ , the calculated form of  $f_+^{D\pi}(t)$  is well described by the monopole fit

$$f_+^{D\pi}(t) = \frac{0.716}{1 - t/m_{\text{mon}}^2}, \quad m_{\text{mon}} = 2.15 \text{ GeV}. \quad (83)$$

A naive vector meson dominance assumption would employ  $m_{\text{mon}} = m_{D^*} = 2.0 \text{ GeV}$ . Using<sup>19</sup>  $|V_{cd}/V_{cs}|^2 = 0.051 \pm 0.002$ ,<sup>1</sup>

$$R_\pi := \frac{Br(D \rightarrow \pi \ell \nu)}{Br(D \rightarrow K \ell \nu)} = 2.47 \left| \frac{V_{cd}}{V_{cs}} \right|^2 = 0.13. \quad (84)$$

The bulk of the  $1/\hat{M}_c$ -corrections cancel in this ratio. Experimentally<sup>1,40,41</sup>

$$R_\pi = \frac{Br(D^0 \rightarrow \pi^- e^+ \nu_e)}{Br(D^0 \rightarrow K^- e^+ \nu_e)} = 0.11_{-0.03}^{+0.06} \pm 0.1, \quad (85)$$

$$R_\pi = 2 \frac{Br(D^+ \rightarrow \pi^0 e^+ \nu_e)}{Br(D^+ \rightarrow \bar{K}^0 e^+ \nu_e)} = 0.17 \pm 0.05 \pm 0.03. \quad (86)$$

If one assumes single-pole,  $D^*$  and  $D_s^*$  vector meson dominance for the  $t$ -dependence of the form factors  $f_+^{D\pi}$  and  $f_+^{DK}$ , one obtains the simple formula

$$R_\pi = 1.97 \left| \frac{f_+^{D\pi}(0)}{f_+^{DK}(0)} \right|^2 \left| \frac{V_{cd}}{V_{cs}} \right|^2. \quad (87)$$

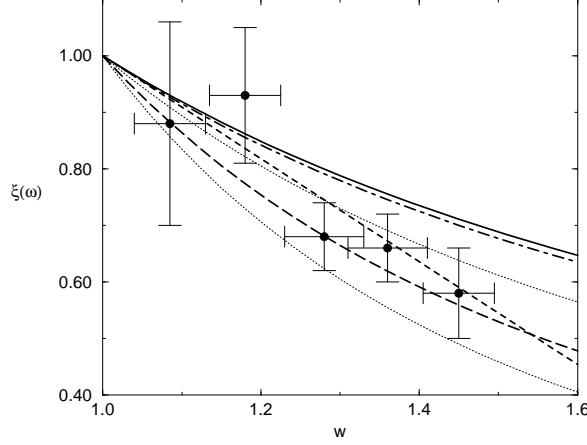


Figure 16: Calculated form of  $\xi(w)$  cf. recent experimental analyses. The solid line was obtained<sup>19</sup> assuming only that the  $b$ -quark is heavy, the dash-dot line assumed the same of the  $c$ -quark. Experiment: data points - Ref. [37]; short-dashed line - linear fit from Ref. [38],  $\xi(w) = 1 - \rho^2 (w - 1)$ ,  $\rho^2 = 0.91 \pm 0.15 \pm 0.16$ ; long-dashed line - nonlinear fit from Ref. [38],  $\xi(w) = [2/(w + 1)] \exp[(1 - 2\rho^2)(w - 1)/(w + 1)]$ ,  $\rho^2 = 1.53 \pm 0.36 \pm 0.14$ . The two light, dotted lines are this nonlinear fit evaluated with the extreme values of  $\rho^2$ : upper line,  $\rho^2 = 1.17$  and lower line,  $\rho^2 = 1.89$ .

That approach was used<sup>1</sup> to estimate  $f_+^{D\pi}(0)/f_+^{DK}(0) = 1.0^{+0.3}_{-0.2} \pm 0.04$  or  $1.3 \pm 0.2 \pm 0.1$  from Eqs. (85) and (86). This calculation<sup>19</sup> yields

$$\frac{f_+^{D\pi}(0)}{f_+^{DK}(0)} = 1.16. \quad (88)$$

It must be noted that Ref. [19] explicitly *did not* assume vector meson dominance. The calculated results reflect only the importance and influence of the dressed-quark and -gluon substructure of the heavy mesons. That substructure is manifest in the dressed propagators and bound state amplitudes, which fully determine the value of every calculated quantity. Explicit vector meson contributions would appear as pole terms in  $\mathcal{V}_\mu^{f_1 f_2}(k_1, k_2)$ , which are excluded in the *Ansatz*:  $\mathcal{V}_\mu^{qQ}(k_1, k_2) = \gamma_\mu$ . That simple-pole *Ansätze* provide efficacious interpolations of the calculated results on the accessible kinematic domain is not surprising, given that the form factor must rise slowly away from its value at  $t = 0$  and the heavy meson mass provides a dominant intrinsic scale, which is only modified slightly by the scale in the light-quark propagators and meson bound state amplitudes. Similar observations are true in the calculation of the

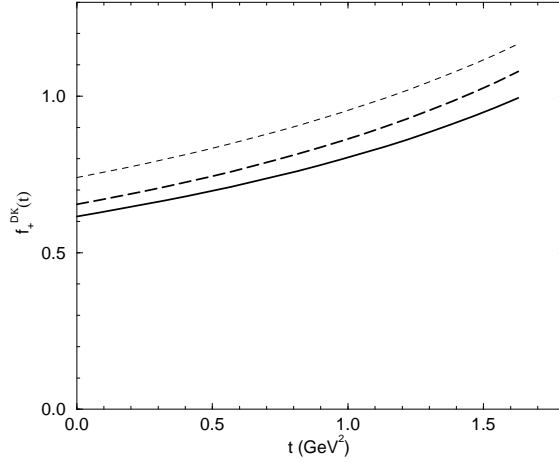


Figure 17: Calculated form of  $f_+^{DK}(q^2)$ : the solid line was obtained<sup>19</sup> assuming only that the  $b$ -quark is heavy, the dashed line assumed the same of the  $c$ -quark. The light, short-dashed line is a vector dominance, monopole model:  $f_+(q^2) = 0.74/(1 - q^2/m_{D_s^*}^2)$ ,  $m_{D_s^*} = 2.11$  GeV.

pion form factor.<sup>23,42</sup>

In this section I illustrated a heavy-quark limit of the DSEs, based on the observation that the mass function of heavy-quarks evolves slowly with momentum, and the manner in which it can be used to describe the properties of heavy-mesons. They are much like light-mesons: bound states of finite extent, with dressed-quark constituents. The analysis of  $B \rightarrow D$ ,  $D \rightarrow K$  and  $D \rightarrow \pi$  transitions indicates that the heavy-quark limit is accurate to within 15-20% for the  $c$ -quark. A significant feature is the correlation of heavy  $\rightarrow$  heavy and heavy  $\rightarrow$  light transitions *and* their correlation with light meson observables, which are dominated by effects such as confinement and DCSB.

## 6 Finite $T$ and $\mu$

Nonperturbative methods are necessary to study the transition to a QGP, which is characterised by qualitative changes in order parameters such as the quark condensate. One widely used approach is the numerical simulation of finite- $T$  lattice-QCD, with the first simulations in the early eighties and extensive efforts since then.<sup>43</sup> They have contributed considerably to the current

understanding of the nature of the QGP. The commonly used quenched approximation is inadequate for studying the phase diagram of finite- $T$  QCD because the details of the transition depend sensitively on the number of active (light) flavours. It is therefore necessary to include the fermion determinant.

That is even more important in the presence of  $\mu$ , which modifies the fermion piece of the Euclidean action:  $\gamma \cdot \partial + m \rightarrow \gamma \cdot \partial - \gamma_4 \mu + m$ , introducing an explicit imaginary part to the fermion determinant. With the  $\mu \neq 0$  lattice-QCD action being complex, the study of finite density is significantly more difficult than that of finite temperature. Simulations that ignore the fermion determinant encounter a forbidden region, which begins at  $\mu = m_\pi/2$ ,<sup>44</sup> and since  $m_\pi \rightarrow 0$  in the chiral limit this is a serious limitation, preventing a reliable study of chiral symmetry restoration. The phase of the fermion determinant is essential in eliminating this artefact.<sup>45</sup>

The contemporary application of DSEs at finite temperature and chemical potential is a straightforward extension of the  $T = 0 = \mu$  studies.<sup>46</sup> The direct approach is to develop a finite- $T$  extension of *Ansätze* for the dressed-gluon propagator. The quark DSE can then be solved and, having the dressed-quark and -gluon propagators, the response of bound states to increases in  $T$  and  $\mu$  can be calculated. As a nonperturbative approach that allows the simultaneous study of confinement and DCSB, the DSEs have a significant overlap with lattice simulations: each quantity that can be estimated using lattice simulations can also be calculated using DSEs. That means they can be used to check the lattice simulations, and importantly, that lattice simulations can be used to constrain their model-dependent aspects. Once agreement is obtained on the common domain, the DSEs can be used to explore phenomena presently inaccessible to lattice simulations.

### 6.1 Finite- $(T, \mu)$ Quark DSE

The renormalised dressed-quark propagator at finite- $(T, \mu)$  has the form

$$S(\vec{p}, \tilde{\omega}_k) = \frac{1}{i\vec{\gamma} \cdot \vec{p} A(\vec{p}, \tilde{\omega}_k) + i\gamma_4 \tilde{\omega}_k C(\vec{p}, \tilde{\omega}_k) + B(\vec{p}, \tilde{\omega}_k)} \quad (89)$$

$$\equiv -i\vec{\gamma} \cdot \vec{p} \sigma_A(\vec{p}, \tilde{\omega}_k) - i\gamma_4 \tilde{\omega}_k \sigma_C(\vec{p}, \tilde{\omega}_k) + \sigma_B(\vec{p}, \tilde{\omega}_k), \quad (90)$$

where  $\tilde{\omega}_k := \omega_k + i\mu$  with  $\omega_k = (2k + 1)\pi T$ ,  $k \in \mathbf{Z}$ , the fermion Matsubara frequencies. The complex scalar functions:  $A(\vec{p}, \tilde{\omega}_k)$ ,  $B(\vec{p}, \tilde{\omega}_k)$  and  $C(\vec{p}, \tilde{\omega}_k)$  satisfy:  $\mathcal{F}(\vec{p}, \tilde{\omega}_k)^* = \mathcal{F}(\vec{p}, \tilde{\omega}_{-k-1})$ ,  $\mathcal{F} = A, B, C$ , and although not explicitly indicated they are functions only of  $|\vec{p}|^2$  and  $\tilde{\omega}_k^2$ . Using the Matsubara<sup>47</sup> (or imaginary-time) formalism  $O(4)$  covariance, the Euclidean realisation of

Poincaré covariance, is broken to  $O(3)$  and only systems in equilibrium can be studied.

$S(\vec{p}, \tilde{\omega}_k)$  satisfies the DSE

$$S^{-1}(\vec{p}, \tilde{\omega}_k) = Z_2^A i\vec{\gamma} \cdot \vec{p} + Z_2 (i\gamma_4 \tilde{\omega}_k + m_{\text{bm}}) + \Sigma'(\vec{p}, \tilde{\omega}_k), \quad (91)$$

where the regularised self energy is

$$\Sigma'(\vec{p}, \tilde{\omega}_k) = i\vec{\gamma} \cdot \vec{p} \Sigma'_A(\vec{p}, \tilde{\omega}_k) + i\gamma_4 \tilde{\omega}_k \Sigma'_C(\vec{p}, \tilde{\omega}_k) + \Sigma'_B(\vec{p}, \tilde{\omega}_k), \quad (92)$$

$$\Sigma'_F(\vec{p}, \tilde{\omega}_k) = \int_{l,q}^{\bar{\Lambda}} \frac{4}{3} g^2 D_{\mu\nu}(\vec{p} - \vec{q}, \tilde{\omega}_k - \tilde{\omega}_l) \frac{1}{4} \text{tr} [\mathcal{P}_F \gamma_\mu S(\vec{q}, \tilde{\omega}_l) \Gamma_\nu(\vec{q}, \tilde{\omega}_l; \vec{p}, \tilde{\omega}_k)] , \quad (93)$$

$\int_{l,q}^{\bar{\Lambda}} := T \sum_{l=-\infty}^{\infty} \int \frac{d^3 q}{(2\pi)^3}$  and  $\mathcal{P}_A := -(Z_1^A/p^2) i\gamma \cdot p$ ,  $\mathcal{P}_B := Z_1$ ,  $\mathcal{P}_C := -(Z_1/\tilde{\omega}_k) i\gamma_4$ . The finite- $(T, \mu)$ , Landau-gauge dressed-gluon propagator in the kernel has the form

$$g^2 D_{\mu\nu}(\vec{p}, \Omega) = P_{\mu\nu}^L(\vec{p}, \Omega) \Delta_F(\vec{p}, \Omega) + P_{\mu\nu}^T(\vec{p}) \Delta_G(p, \Omega), \quad (94)$$

$$P_{\mu\nu}^T(\vec{p}) := \begin{cases} 0; & \mu \text{ and/or } \nu = 4, \\ \delta_{ij} - \frac{p_i p_j}{|\vec{p}|^2}; & \mu, \nu = i, j = 1, 2, 3 \end{cases} , \quad (95)$$

with  $P_{\mu\nu}^T(p) + P_{\mu\nu}^L(p, p_4) = \delta_{\mu\nu} - p_\mu p_\nu / (\sum_{\alpha=1}^4 p_\alpha p_\alpha)$ ;  $\mu, \nu = 1, \dots, 4$ .

Whether or not  $(T, \mu)$  are nonzero, in studying confinement one cannot assume that the analytic structure of a dressed propagator is the same as that of the free particle propagator: it must be determined dynamically. The  $\tilde{p}_k := (\vec{p}, \tilde{\omega}_k)$ -dependence of  $A$  and  $C$  is qualitatively important since it can conspire with that of  $B$  to eliminate free-particle poles in the dressed-quark propagator.<sup>48</sup> In that case the propagator does not have a Lehmann representation so that, in general, the Matsubara sum cannot be evaluated analytically. More importantly, it further complicates a real-time formulation of the finite temperature theory making the study of nonequilibrium thermodynamics a very challenging problem. In addition, the  $\tilde{p}_k$ -dependence of  $A$  and  $C$  can be a crucial factor in determining the behaviour of bulk thermodynamic quantities such as the pressure and entropy, being responsible for these quantities reaching their respective ultrarelativistic limits only for very large values of  $T$  and  $\mu$ . It is therefore important in any DSE study to retain  $A(\tilde{p}_k)$  and  $C(\tilde{p}_k)$ , and their dependence on  $\tilde{p}_k$ .

## 6.2 Phase Transitions and Order Parameters

One order parameter for the chiral symmetry restoration transition is the quark condensate, defined via the renormalised dressed-quark propagator, Eq. (36). An equivalent order parameter is

$$\mathcal{X} := \text{Re } B_0(\vec{p}=0, \tilde{\omega}_0), \quad (96)$$

which makes it clear that the zeroth Matsubara mode determines the character of the chiral phase transition. An order parameter for confinement, valid for both light- and heavy-quarks, was introduced in Ref. [49]. It is a single, quantitative measure of whether or not a Schwinger function has a Lehmann representation, and has been used<sup>50</sup> to striking effect in QED<sub>3</sub>.

## 6.3 Study at $(T \neq 0, \mu = 0)$

Deconfinement and chiral symmetry restoration at  $T \neq 0$  have been studied<sup>49</sup> in a DSE-model of two-light-flavour QCD. The quark DSE was solved using a one-parameter model dressed-gluon propagator, which provides a good description of  $\pi$  and  $\rho$ -meson observables at  $T = 0 = \mu$ .<sup>51</sup> The transitions are coincident and second-order at a critical temperature of  $T_c \approx 150$  MeV, with the same estimated critical exponents:  $\beta = 0.33 \pm 0.03$ . Both  $m_\pi$  and  $f_\pi$  are insensitive to  $T$  for  $T \lesssim 0.7 T_c$ . The evolution with  $T$  is so slow that even at  $T = 0.9 T_c$  there is only a 20% suppression of  $\Gamma_{\pi \rightarrow \ell \nu}$ . However, for  $T$  very near to  $T_c$  the pion mass increases substantially, as thermal fluctuations overwhelm quark-antiquark attraction in the pseudoscalar channel, until, at  $T = T_c$ ,  $f_\pi \rightarrow 0$  and there is no bound state. These results confirm<sup>9</sup> those of contemporary numerical simulations of finite- $T$  lattice-QCD.<sup>43</sup>

## 6.4 Complementary study at $(T = 0, \mu \neq 0)$

The behaviour of this model at  $\mu \neq 0$  has also been explored.<sup>55</sup> Using the simple dressed-gluon propagator<sup>51</sup>

$$\frac{\mathcal{G}(k^2)}{k^2} = \frac{16}{9} \pi^2 \left[ 4\pi^2 m_t^2 \delta^4(k) + \frac{1 - e^{-[k^2/(4m_t^2)]}}{k^2} \right], \quad (97)$$

---

<sup>9</sup>The lattice and DSE estimates of  $\beta_{\mathcal{X}}$ , however, do not survive more exhaustive studies,<sup>52,53</sup> and the most recent analyses<sup>53,54</sup> suggest that in DSE models whose long-range part is described by a  $\delta$ -function singularity the chiral symmetry restoration transition at finite- $T$  is described by a mean-field value of  $\beta$ .

where  $m_t = 0.69 \text{ GeV} = 1/[0.29 \text{ fm}]$  is a mass-scale that marks the boundary between the perturbative and nonperturbative domains, the quark DSE was solved in rainbow approximation. The solution has the form

$$S(p_{[\mu]}) := -i\vec{\gamma} \cdot \vec{p} \sigma_A(p_{[\mu]}) - i\gamma_4 \omega_{[\mu]} \sigma_C(p_{[\mu]}) + \sigma_B(p_{[\mu]}), \quad (98)$$

where  $p_{[\mu]} := (\vec{p}, \omega_{[\mu]})$ , with  $\omega_{[\mu]} := p_4 + i\mu$ .

As elucidated in Sec. 6.5, there are two distinct types of solution: a Nambu-Goldstone mode with confinement and DCSB characterised by  $\sigma_{B_0} \neq 0$ ; and a deconfined, chirally-symmetric Wigner-Weyl mode characterised by  $\sigma_{B_0} \equiv 0$ . The possibility of a phase transition between the two modes is explored by calculating the relative stability of the different phases, which is measured by the difference between their tree-level auxiliary-field effective-actions:

$$\frac{1}{2N_f N_c} \mathcal{B}(\mu) := \int^\Lambda \frac{d^4 p}{(2\pi)^4} \quad (99)$$

$$\left\{ \ln \left[ \frac{|\vec{p}|^2 A_0^2 + \omega_{[\mu]}^2 C_0^2 + B_0^2}{|\vec{p}|^2 \hat{A}_0^2 + \omega_{[\mu]}^2 \hat{C}_0^2} \right] + |\vec{p}|^2 (\sigma_{A_0} - \hat{\sigma}_{A_0}) + \omega_{[\mu]}^2 (\sigma_{C_0} - \hat{\sigma}_{C_0}) \right\},$$

where  $\hat{A}$  and  $\hat{C}$  represent the solution of Eq. (91) obtained when  $B_0 \equiv 0$ ; i.e., when DCSB is absent. This solution exists for all  $\mu$ .  $\mathcal{B}(\mu)$  defines a  $\mu$ -dependent “bag constant”.<sup>56</sup> It is positive when the Nambu-Goldstone phase is dynamically favoured; i.e., has the highest pressure, and becomes negative when the Wigner pressure becomes larger. Hence the critical chemical potential is the zero of  $\mathcal{B}(\mu)$ , which is  $\mu_c = 375 \text{ MeV}$ . The abrupt switch from the Nambu-Goldstone to the Wigner-Weyl mode signals a first order transition.

The chiral order parameter *increases* with increasing chemical potential up to  $\mu_c$ , with  $\mathcal{X}(\mu_c)/\mathcal{X}(0) \approx 1.2$ , whereas the deconfinement order parameter,  $\kappa(\mu)$ , is insensitive to increasing  $\mu$ . At  $\mu_c$  they both drop immediately and discontinuously to zero, as expected of coincident, first-order phase transitions. The increase of  $\mathcal{X}$  with  $\mu$  is a necessary consequence of the momentum dependence of the scalar piece of the quark self energy,  $B(p_{[\mu]})$ .<sup>57</sup> The vacuum quark condensate behaves in qualitatively the same manner as  $\mathcal{X}$ .

Even though the chiral order parameter *increases* with  $\mu$ ,  $m_\pi$  *decreases* slowly as  $\mu$  increases, with  $m_\pi(\mu \approx 0.7 \mu_c)/m_\pi(0) \approx 0.94$ . At this point  $m_\pi$  begins to increase although, for  $\mu < \mu_c$ ,  $m_\pi(\mu)$  does not exceed  $m_\pi(0)$ , which precludes pion condensation. The behaviour of  $m_\pi$  results from mutually compensating increases in  $f_\pi^2$  and  $\langle m_R^\zeta(\bar{q}q)_\zeta \rangle_\pi$ .  $f_\pi$  is insensitive to the chemical potential until  $\mu \approx 0.7 \mu_c$ , when it increases sharply so that  $f_\pi(\mu_c^-)/f_\pi(\mu = 0) \approx 1.25$ . The relative insensitivity of  $m_\pi$  and  $f_\pi$  to changes in  $\mu$ , until very



near  $\mu_c$ , mirrors the behaviour of these observables at finite- $T$ .<sup>49</sup> For example, it leads only to a 14% change in  $\Gamma_{\pi \rightarrow \mu \nu}$  at  $\mu \approx 0.9\mu_c$ : an *increase* in this case. The universal scaling conjecture of Ref. [58] is inconsistent with the anticorrelation observed between the  $\mu$ -dependence of  $f_\pi$  and  $m_\pi$ .

**6.4.1:  $\mu$ -dependence anticorrelated with  $T$ -dependence.** Comparing the  $\mu$ -dependence of  $f_\pi$  and  $m_\pi$  with their  $T$ -dependence, one observes an anticorrelation; e.g., at  $\mu = 0$ ,  $f_\pi$  falls continuously to zero as  $T$  is increased towards  $T_c \approx 150$  MeV. This is a necessary consequence of the momentum-dependence of the quark self energy. In calculating these observables one obtains expressions for  $m_\pi^2$  or  $f_\pi^2$  and thus the natural dimension is mass-squared. Therefore their behaviour at finite  $T$  and  $\mu$  is determined by

$$\text{Re}(\omega_{[\mu]}^2) \sim [\pi^2 T^2 - \mu^2], \quad (100)$$

where the  $T$ -dependence arises from the introduction of the fermion Matsubara frequency:  $p_4 \rightarrow (2k+1)\pi T$ . Hence when such a quantity decreases with  $T$  it will increase with  $\mu$ , and vice-versa.<sup>59</sup>

**6.4.2:  $(-\langle \bar{q}q \rangle)$  increases with  $\mu$ .** The confined-quark vacuum consists of quark-antiquark pairs correlated in a scalar condensate and increasing  $\mu$  increases the scalar density:  $(-\langle \bar{q}q \rangle)$ . This is an expected consequence of confinement, which entails that each additional quark must be locally paired with an antiquark thereby increasing the density of condensate pairs as  $\mu$  is increased. For this reason, as long as  $\mu < \mu_c$ , there is no excess of particles over antiparticles *in the vacuum* and hence the baryon number density remains zero,<sup>57</sup> i.e.,  $\rho_B^{u+d} = 0$ ,  $\mu < \mu_c$ . This is just the statement that quark-antiquark pairs confined in the condensate do not contribute to the baryon number density.

**6.4.3: The core of neutron stars.** The vacuum quark pressure,  $P^{u+d}[\mu]$ , can be calculated.<sup>57</sup> After deconfinement it increases rapidly, as the condensate “breaks-up”, and an excess of quarks over antiquarks develops. The baryon-number density,  $\rho_B^{u+d} = (1/3)\partial P^{u+d}/\partial\mu$ , also increases rapidly, with

$$\rho_B^{u+d}(\mu \approx 2\mu_c) \simeq 3\rho_0, \quad (101)$$

where  $\rho_0 = 0.16 \text{ fm}^{-3}$  is the equilibrium density of nuclear matter. For comparison, the central core density expected in a  $1.4 M_\odot$  neutron star is  $3.6\text{--}4.1 \rho_0$ .<sup>60</sup> Finally, at  $\mu \sim 5\mu_c$ , the quark pressure saturates the ultrarelativistic limit:  $P^{u+d} = \mu^4/(2\pi^2)$ , and there is a simple relation between baryon-density and chemical-potential:

$$\rho_B^{u_F+d_F}(\mu) = \frac{1}{3} \frac{2\mu^3}{\pi^2}, \quad \forall \mu \gtrsim 5\mu_c, \quad (102)$$

so that  $\rho_B^{u_F+d_F}(5\mu_c) \sim 350 \rho_0$ . Thus the quark pressure in the deconfined domain overwhelms any finite, additive contribution of hadrons to the equation of state. That was anticipated in Ref. [55] where the hadron contribution was neglected. This discussion suggests that a QGP is likely to exist in the core of dense neutron stars.

### 6.5 Simultaneous study of $(T \neq 0, \mu \neq 0)$

This is a difficult problem and the most complete study<sup>57</sup> to date employs a simple *Ansatz* for the dressed-gluon propagator that exhibits the infrared enhancement suggested by Ref. [17]:

$$g^2 D_{\mu\nu}(\vec{p}, \Omega_k) = \left( \delta_{\mu\nu} - \frac{p_\mu p_\nu}{|\vec{p}|^2 + \Omega_k^2} \right) 2\pi^3 \frac{\eta^2}{T} \delta_{k0} \delta^3(\vec{p}), \quad (103)$$

with  $\Omega_k = 2k\pi T$ , the boson Matsubara frequency. As an infrared-dominant model that does not represent well the behaviour of  $D_{\mu\nu}(\vec{p}, \Omega_k)$  away from  $|\vec{p}|^2 + \Omega_k^2 \approx 0$ , some model-dependent artefacts arise. However, there is significant merit in its simplicity and, since the artefacts are easily identified, the model remains useful as a means of elucidating many of the qualitative features of more sophisticated *Ansätze*.

With this model, using the rainbow approximation, the quark DSE is<sup>13</sup>

$$S^{-1}(\vec{p}, \omega_k) = S_0^{-1}(\vec{p}, \tilde{\omega}_k) + \frac{1}{4} \eta^2 \gamma_\nu S(\vec{p}, \tilde{\omega}_k) \gamma_\nu. \quad (104)$$

A simplicity inherent in Eq. (103) is now apparent: it allows the reduction of an integral equation to an algebraic equation, in whose solution many of the qualitative features of more sophisticated models are manifest.

In the chiral limit Eq. (104) reduces to a quadratic equation for  $B(\tilde{p}_k)$ , which has two qualitatively distinct solutions. The Nambu-Goldstone solution, with

$$B(\tilde{p}_k) = \begin{cases} \sqrt{\eta^2 - 4\tilde{p}_k^2}, & \text{Re}(\tilde{p}_k^2) < \frac{\eta^2}{4}, \\ 0, & \text{otherwise} \end{cases}, \quad (105)$$

$$C(\tilde{p}_k) = \begin{cases} 2, & \text{Re}(\tilde{p}_k^2) < \frac{\eta^2}{4}, \\ \frac{1}{2} \left( 1 + \sqrt{1 + \frac{2\eta^2}{\tilde{p}_k^2}} \right), & \text{otherwise} \end{cases}, \quad (106)$$

describes a phase of this model in which: 1) chiral symmetry is dynamically broken, because one has a nonzero quark mass-function,  $B(\tilde{p}_k)$ , in the absence

of a current-quark mass; and 2) the dressed-quarks are confined, because the propagator described by these functions does not have a Lehmann representation. The alternative Wigner solution, for which

$$\hat{B}(\tilde{p}_k) \equiv 0, \quad \hat{C}(\tilde{p}_k) = \frac{1}{2} \left( 1 + \sqrt{1 + \frac{2\eta^2}{\tilde{p}_k^2}} \right), \quad (107)$$

describes a phase of the model with neither DCSB nor confinement. Here the relative stability of the different phases is measured by a  $(T, \mu)$ -dependent vacuum pressure difference; i.e., a  $(T, \mu)$ -dependent bag constant:  $\mathcal{B}(T, \mu)$ .

$\mathcal{B}(T, \mu) = 0$  defines the phase boundary, and the deconfinement and chiral symmetry restoration transitions are coincident. For  $\mu = 0$  the transition is second order and the critical temperature is  $T_c^0 = 0.159\eta$ , which using the value of  $\eta = 1.06$  GeV obtained by fitting the  $\pi$  and  $\rho$  masses corresponds to  $T_c^0 = 0.170$  GeV. This is only 12% larger than the value reported in Sec. 6.3, and the order of the transition is the same. For any  $\mu \neq 0$  the transition is first-order. For  $T = 0$  the critical chemical potential is  $\mu_c^0 = 0.3$  GeV, which is  $\approx 30\%$  smaller than the result in Sec. 6.4. The discontinuity in the order parameter vanishes at  $\mu = 0$ , and this defines a tricritical point.

In this model the quark pressure,  $P_q$ , is calculated easily. Confinement means that  $P_q \equiv 0$  in the confined domain. In the deconfined domain it approaches the ultrarelativistic, free particle limit,  $P_{UR}$ , at large values of  $T$  and  $\mu$ . However, the approach to this limit is slow. For example, at  $T \sim 0.3\eta \sim 2T_c^0$ , or  $\mu \sim \eta \sim 3\mu_c^0$ ,  $P_q$  is only  $0.5 P_{UR}$ . A qualitatively similar result is observed in numerical simulations of finite- $T$  lattice-QCD.<sup>43</sup> This feature results from the persistence of momentum dependent modifications of the quark propagator into the deconfined domain, as evident with  $C \neq 1$  in Eq. (107). It predicts a “mirroring” of finite- $T$  behaviour in the  $\mu$ -dependence of the bulk thermodynamic quantities, as illustrated in Fig. 18.

### 6.6 $\pi$ and $\rho$ properties

The model introduced in the last section has also been used<sup>59</sup> to study the  $(T, \mu)$ -dependence of meson properties, and to elucidate other features of models that employ a more sophisticated *Ansatz* for the dressed-gluon propagator. For example, the vacuum quark condensate is given by the simple expression

$$-\langle \bar{q}q \rangle = \eta^3 \frac{8N_c}{\pi^2} \bar{T} \sum_{l=0}^{l_{\max}} \int_0^{\bar{\Lambda}_l} dy y^2 \operatorname{Re} \left( \sqrt{\frac{1}{4} - y^2 - \bar{\omega}_l^2} \right), \quad (108)$$

$\bar{T} = T/\eta$ ,  $\bar{\mu} = \mu/\eta$ ;  $l_{\max}$  is the largest value of  $l$  for which  $\bar{\omega}_{l_{\max}}^2 \leq (1/4) + \bar{\mu}^2$  and this also specifies  $\omega_{l_{\max}}$ ,  $\bar{\Lambda}^2 = \bar{\omega}_{l_{\max}}^2 - \bar{\omega}_l^2$ ,  $\bar{p}_l = (\vec{y}, \bar{\omega}_l + i\bar{\mu})$ . At  $T = 0 = \mu$ ,

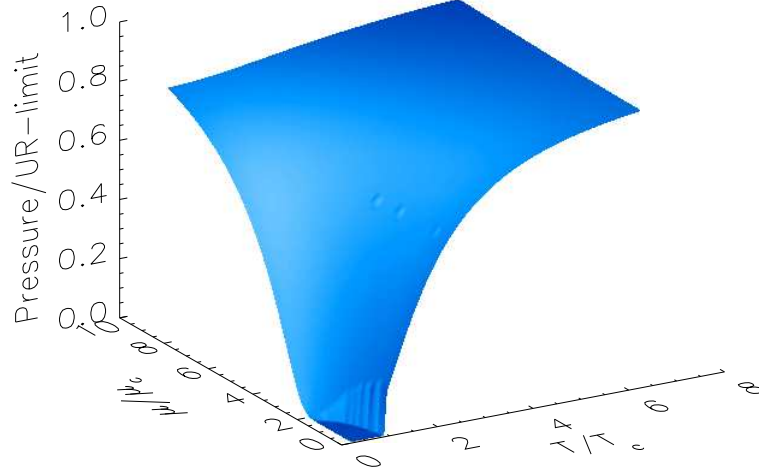


Figure 18: The quark pressure,  $P_q(\bar{T}, \bar{\mu})$ , normalised to the free, massless (or Ultra-Relativistic) result.

$(-\langle \bar{q}q \rangle) = \eta^3 / (80 \pi^2) = (0.11 \eta)^3$ . Obvious from Eq. (108) is that  $(-\langle \bar{q}q \rangle)$  decreases continuously to zero with  $T$  but *increases* with  $\mu$ , up to a critical value of  $\mu_c(T)$  when it drops discontinuously to zero: behaviour in agreement with that reported in Secs. 6.3 and 6.4. The vacuum rearrangement emphasised in Sec. 6.4.2 is manifest in the behaviour of the necessarily-momentum-dependent scalar part of the quark self energy,  $B(\tilde{p}_k)$  in Eq. (105).

The leptonic decay constant is also given by a simple expression in the chiral limit:

$$f_\pi^2 = \eta^2 \frac{16 N_c}{\pi^2} \bar{T} \sum_{l=0}^{l_{\max}} \frac{\bar{\Lambda}_l^3}{3} \left( 1 + 4 \bar{\mu}^2 - 4 \bar{\omega}_l^2 - \frac{8}{5} \bar{\Lambda}_l^2 \right). \quad (109)$$

As anticipated, the combination  $\mu^2 - \omega_l^2$ , emphasised in Sec. 6.4.1, characterises the behaviour of Eqs. (108) and (109). Without calculation, Eq. (109) indicates that  $f_\pi$  will *decrease* with  $T$  and *increase* with  $\mu$ , which provides a simple elucidation of the results in Secs. 6.3 and 6.4

The  $(T, \mu)$ -response of meson masses is determined by the ladder BSE

$$\Gamma_M(\tilde{p}_k; \tilde{P}_\ell) = -\frac{\eta^2}{4} \text{Re} \left\{ \gamma_\mu S(\tilde{p}_i + \frac{1}{2} \tilde{P}_\ell) \Gamma_M(\tilde{p}_i; \tilde{P}_\ell) S(\tilde{p}_i - \frac{1}{2} \tilde{P}_\ell) \gamma_\mu \right\}, \quad (110)$$

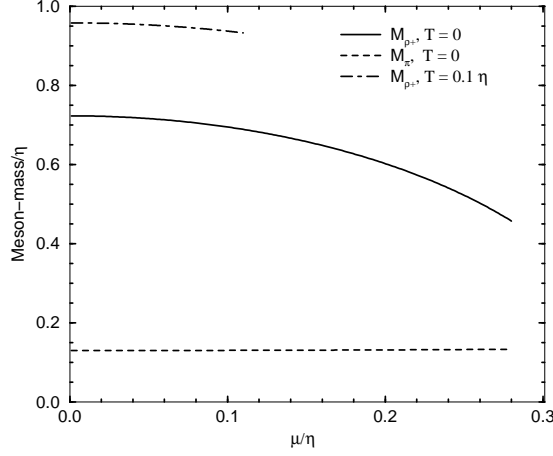


Figure 19:  $M_{\rho+} = M_{\omega+}$  and  $M_{\pi}$  as a function of  $\bar{\mu}$  for  $\bar{T} = 0, 0.1$ . On the scale of this figure,  $M_{\pi}$  is insensitive to this variation of  $T$ . The current-quark mass is  $m = 0.011 \eta$ , which for  $\eta = 1.06 \text{ GeV}$  yields  $M_{\rho+} = 770 \text{ MeV}$  and  $M_{\pi} = 140 \text{ MeV}$  at  $T = 0 = \mu$ .

where  $\tilde{P}_{\ell} := (\vec{P}, \Omega_{\ell})$ , with the bound state mass obtained by considering  $\tilde{P}_{\ell=0}$ . In this truncation the  $\omega$ - and  $\rho$ -mesons are degenerate.

The equation admits a solution for the  $\pi$ -meson with

$$\Gamma_{\pi}(P_0) = \gamma_5 \left( i\theta_1 + \vec{\gamma} \cdot \vec{P} \theta_2 \right) \quad (111)$$

and the calculated  $(T, \mu)$ -dependence of the mass is depicted in Fig. 19.

For the  $\rho$ -meson the solution has two components: one longitudinal and one transverse to  $\vec{P}$ . The solution of the BSE has the form

$$\Gamma_{\rho} = \left\{ \begin{array}{l} \gamma_4 \theta_{\rho+} \\ \left( \vec{\gamma} - \frac{1}{|\vec{P}|^2} \vec{P} \vec{\gamma} \cdot \vec{P} \right) \theta_{\rho-} \end{array} \right. , \quad (112)$$

where  $\theta_{\rho+}$  labels the longitudinal and  $\theta_{\rho-}$  the transverse solution. The eigenvalue equation obtained from Eq. (110) for the bound state mass,  $M_{\rho\pm}$ , is

$$\frac{\eta^2}{2} \text{Re} \left\{ \sigma_S (\omega_{0+}^2 - \frac{1}{4} M_{\rho\pm}^2)^2 - \left[ \pm \omega_{0+}^2 - \frac{1}{4} M_{\rho\pm}^2 \right] \sigma_V (\omega_{0+}^2 - \frac{1}{4} M_{\rho\pm}^2)^2 \right\} = 1. \quad (113)$$

The mass of the transverse component is obtained with  $[-\omega_{0+}^2 - (1/4)M_{\rho-}^2]$  in Eq. (113). Using the chiral-limit solutions, Eq. (105), one obtains immedi-

ately that

$$M_{\rho-}^2 = \frac{1}{2}\eta^2, \text{ independent of } T \text{ and } \mu. \quad (114)$$

Even for nonzero current-quark mass,  $M_{\rho-}$  changes by less than 1% as  $T$  and  $\mu$  are increased from zero toward their critical values. Its insensitivity is consistent with the absence of a constant mass-shift in the transverse polarisation tensor for a gauge-boson.

For the longitudinal component one obtains in the chiral limit:

$$M_{\rho+}^2 = \frac{1}{2}\eta^2 - 4(\mu^2 - \pi^2 T^2). \quad (115)$$

The characteristic combination  $\mu^2 - \pi^2 T^2$  again indicates the anticorrelation between the response of  $M_{\rho+}$  to  $T$  and its response to  $\mu$ , and, like a gauge-boson Debye mass, that  $M_{\rho+}^2$  rises linearly with  $T^2$  for  $\mu = 0$ . The  $m \neq 0$  solution of Eq. (113) for the longitudinal component is plotted in Fig. 19:  $M_{\rho+}$  increases with increasing  $T$  and decreases as  $\mu$  increases.

Equation (113) can also be applied to the  $\phi$ -meson. The transverse component is insensitive to  $T$  and  $\mu$ , and the behaviour of the longitudinal mass,  $M_{\phi+}$ , is qualitatively the same as that of the  $\rho$ -meson: it increases with  $T$  and decreases with  $\mu$ . Using  $\eta = 1.06$  GeV, this simple model yields  $M_{\phi\pm} = 1.02$  GeV for  $m_s = 180$  MeV at  $T = 0 = \mu$ .

In a 2-flavour, free-quark gas at  $T = 0$  the baryon number density is  $\rho_B = 2\mu^3/(3\pi^2)$ , by which gauge nuclear matter density,  $\rho_0 = 0.16 \text{ fm}^{-3}$ , corresponds to  $\mu = \mu_0 := 260 \text{ MeV} = 0.245 \eta$ . At this chemical potential the algebraic model yields

$$M_{\rho+}(\mu_0) \approx 0.75 M_{\rho+}(\mu = 0), \quad M_{\phi+}(\mu_0) \approx 0.85 M_{\phi+}(\mu = 0). \quad (116)$$

The study summarised in Sec. 6.4 indicates that a better representation of the ultraviolet behaviour of the dressed-gluon propagator expands the horizontal scale in Fig. 19, with the critical chemical potential increased by 25%. This suggests that a more realistic estimate is obtained by evaluating the mass at  $\mu'_0 = 0.20 \eta$ , which yields

$$M_{\rho+}(\mu'_0) \approx 0.85 M_{\rho+}(\mu = 0), \quad M_{\phi+}(\mu'_0) \approx 0.90 M_{\phi+}(\mu = 0); \quad (117)$$

a small, quantitative modification. The difference between Eqs. (116) and (117) is a measure of the theoretical uncertainty in the estimates in each case. Pursuing this suggestion further,  $\mu = \sqrt[3]{2} \mu'_0$ , corresponds to  $2\rho_0$ , at which point  $M_{\omega+} = M_{\rho+} \approx 0.72 M_{\rho+}(\mu = 0)$  and  $M_{\phi+} \approx 0.85 M_{\phi+}(\mu = 0)$ , while at the  $T = 0$  critical chemical potential, which corresponds to approximately  $3\rho_0$

in Sec. 6.4,  $M_{\omega+} = M_{\rho+} \approx 0.65 M_{\rho+}(\mu = 0)$  and  $M_{\phi+} \approx 0.80 M_{\phi+}(\mu = 0)$ . These are the maximum possible reductions in the meson masses.

This simple model preserves the momentum-dependence of gluon and quark dressing, which is an important qualitative feature of more sophisticated studies. Its simplicity means that many of the consequences of that dressing can be demonstrated algebraically. For example, it elucidates the origin of an anticorrelation, highlighted in Sec. 6.4.1 and found for a range of quantities, between their response to increasing  $T$  and that to increasing  $\mu$ . That makes clear why the transition to a QGP is second order with increasing  $T$  and first order with  $\mu$ . Further, in providing an algebraic explanation of why the  $(T, \mu)$ -dependence of  $(-\langle \bar{q}q \rangle)$  and  $f_\pi$  is opposite to that observed for  $M_{\rho+}$ , it emphasises that the scaling law conjectured in Ref. [58] is inconsistent with many actual calculations that preserve the global symmetries of QCD.

## 7 Some Final Remarks

There are many challenges in hadronic physics and I have only presented an outline here. What should be clear, however, is that this field is prescribed by the need for nonperturbative methods *and* models. The models are necessary to propagate the qualitatively robust results of difficult nonperturbative studies into that realm where comparison with the current and future generation of experiments is possible.

The DSEs serve both purposes: they provide a nonperturbative tool and a model framework, and have been used widely and efficaciously. In addition to the exemplars described herein, there are many other recent studies. Some are reviewed in Ref. [42], others are a calculation of the cross sections for diffractive, vector meson electroproduction,<sup>61</sup> the electric dipole moment of the  $\rho$ -meson,<sup>62</sup> and an exploration of  $\eta$ - $\eta'$  mixing.<sup>63</sup>

There are two key phenomenological aspects of contemporary DSE applications: modelling the infrared behaviour of the gluon propagator and truncating the kernel of the Bethe-Salpeter equation. They introduce a model-dependence, which is restricted to the infrared because the weak-coupling expansion reproduces perturbation theory and hence the  $k^2 \gtrsim 1 \text{ GeV}^2$  behaviour is fixed in both cases.

As always, one should maintain a constructive scepticism about the fidelity of model input. Its impact must be gauged; e.g., by exploring and exploiting the constraints that Ward Identities and Slavnov-Taylor identities can provide in the theory. That approach has been particularly fruitful in QED<sup>15</sup> and already in the development<sup>13</sup> of a systematic truncation procedure for the kernel of the BSE in QCD.

Such checks are a useful adjunct. However, widespread phenomenological applications remain a key. Pushing a single framework, successful on a large domain, to its limits is a very effective means of identifying which elements of the approach need improvement, and an excellent way to focus resources on those sites requiring further, fundamental developments.

### Acknowledgments

I am grateful to the staff of the National Centre for Theoretical Physics at the Australian National University for their hospitality and support during the summer school. This work was supported by the US Department of Energy, Nuclear Physics Division, under contract no. W-31-109-ENG-38.

### References

1. Particle Data Group (R. M. Barnett *et al.*), *Phys. Rev. D* **54**, 1 (1996).
2. S. Kopecki, *et al.*, *Phys. Rev. Lett.* **70**, 2427 (1995).
3. C. J. Burden, C. D. Roberts and M. J. Thomson, *Phys. Lett. B* **371**, 163 (1996).
4. F. T. Hawes and M. A. Pichowsky, “Electromagnetic form factors of light vector mesons”, nucl-th/9806025.
5. W. R. Molzon, *et al.*, *Phys. Rev. Lett.* **41**, 1213 (1978).
6. D. Drechsel, *et al.*, “Hadron Polarizabilities and Form Factors”, nucl-th/9712013.
7. J. C. Collins and M. J. Perry, *Phys. Rev. Lett.* **34**, 1353 (1975).
8. <http://www.desy.de/>
9. <http://www.cebaf.gov/>
10. <http://www.lns.cornell.edu/>
11. <http://www.bnl.gov/>
12. <http://www.cern.ch/>
13. A. Bender, C. D. Roberts and L. v. Smekal, *Phys. Lett. B* **380**, 7 (1996)
14. C. D. Roberts in *Quark Confinement and the Hadron Spectrum II*, edited by N. Brambilla and G. M. Prosperi (World Scientific, Singapore, 1997), pp. 224-230.
15. A. Bashir, A. Kizilersu and M.R. Pennington, *Phys. Rev. D* **57**, 1242 (1998); and references therein.
16. C. D. Roberts and A. G. Williams, *Prog. Part. Nucl. Phys.* **33**, 477 (1994).
17. N. Brown and M.R. Pennington, *Phys. Rev. D* **39**, 2723 (1989);  
M. R. Pennington, “Calculating hadronic properties in strong QCD”,



- hep-ph/9611242; and references therein.
18. P. Maris and C. D. Roberts, *Phys. Rev. C* **56**, 3369 (1997).
  19. M. A. Ivanov, Yu. Kalinovsky, P. Maris and C. D. Roberts, *Phys. Rev. C* **57**, 1991 (1998).
  20. H. J. Munczek and A. M. Nemirovsky, *Phys. Rev. D* **28**, 181 (1983).
  21. D. B. Leinweber, *Ann. Phys.* **254**, 328 (1997).
  22. P. Maris and C. D. Roberts, “Pseudovector components of the pion,  $\pi^0 \rightarrow \gamma\gamma$ , and  $F_\pi(q^2)$ ”: nucl-th/9804062.
  23. C. D. Roberts, *Nucl. Phys. A* **605**, 475 (1996).
  24. P. Maris and C. D. Roberts in *Rostock 1997, Progress in heavy quark physics*, edited by M. Beyer, T. Mannel and H. Schröder, pp. 159-162; nucl-th/9710062.
  25. N. Isgur and M. B. Wise, *Phys. Lett. B* **237**, 527 (1990).
  26. UKQCD Coll. (D. R. Burford *et al.*), *Nucl. Phys. B* **447**, 425 (1995).
  27. CLEO Coll. (J. P. Alexander *et al.*), *Phys. Rev. Lett.* **77**, 5000 (1996).
  28. J. M. Flynn and C. T. Sachrajda, “Heavy Quark Physics From Lattice QCD”, hep-lat/9710057.
  29. L. Lellouch, *Nucl. Phys. B* **479**, 353 (1996).
  30. M. Wirbel, B. Stech and M. Bauer, *Z. Phys. C* **29**, 637 (1985).
  31. R. N. Faustov, V. O. Galkin and A. Yu. Mishurov, *Phys. Lett. B* **356**, 516 (1995).
  32. N.B. Demchuk, I.L. Grach, I.M. Narodetski and S. Simula, *Phys. Atom. Nucl.* **59**, 2152 (1996).
  33. V. M. Belyaev, V. M. Braun, A. Khodjamirian and R. Rückl, *Phys. Rev. D* **51**, 6177 (1995).
  34. M. A. Ivanov, O. E. Khomutenko and T. Mitzutani, *Phys. Rev. D* **46**, 3817 (1992).
  35. M. A. Ivanov and Yu. M. Valit, *Mod. Phys. Lett. A* **12**, 653 (1997).
  36. M. A. Ivanov and Yu. M. Valit, “Heavy-to-light form factors in the quark model with heavy infrapropagators”, hep-ph/9606404, to appear in *Few-Body Syst.*
  37. ARGUS Collaboration, *Z. Phys. C* **57**, 249 (1993).
  38. CLEO Coll. (J.E. Duboscq *et al.*), *Phys. Rev. Lett.* **76**, 3899 (1996).
  39. J. Richman, in the proceedings of the *28th International Conference on High Energy Physics*, Warsaw, Poland, 25-31 July 1996, ed. Z. Ajduk and A. K. Wroblewski (World Scientific, Singapore, 1997) 143.
  40. MARK III Coll. (J. Adler *et al.*), *Phys. Rev. Lett.* **62**, 1821 (1989).
  41. CLEO Coll. (M. S. Alam *et al.*), *Phys. Rev. Lett.* **71**, 1311 (1993).
  42. P. C. Tandy, *Prog. Part. Nucl. Phys.* **39**, 117 (1997).
  43. F. Karsch, *Nucl. Phys. A* **590**, 376c (1995).

44. M.-P. Lombardo, J. B. Kogut and D. K. Sinclair, *Phys. Rev. D* **54**, 2303 (1996).
45. M. A. Halasz, A. D. Jackson and J. J. M. Verbaarschot, *Phys. Rev. D* **56**, 5140 (1997).
46. C. D. Roberts, in *Light-Front Quantization and Non-Perturbative QCD*, edited by J. P. Vary and F. Wölz (International Institute of Theoretical and Applied Physics, Ames, 1997) pp. 212-239:  
<http://www.iitap.iastate.edu/reports/lfw/contents.html>.
47. R. J. Rivers, *Path integral methods in quantum field theory*, Cambridge University Press, Cambridge, UK (1987).
48. C. J. Burden, C. D. Roberts and A. G. Williams, *Phys. Lett. B* **285**, 347 (1992).
49. A. Bender, D. Blaschke, Yu. Kalinovsky and C.D. Roberts, *Phys. Rev. Lett.* **77**, 3724 (1996).
50. P. Maris, *Phys. Rev. D* **52**, 6087 (1995).
51. M. R. Frank and C. D. Roberts, *Phys. Rev. C* **53**, 390 (1996).
52. E. Laermann, “Thermodynamics using Wilson and Staggered Quarks”, hep-lat/9802030.
53. D. Blaschke, A. Hoell, C. D. Roberts and S. Schmidt, “Analysis of chiral and thermal susceptibilities”, nucl-th/9803030, *Phys. Rev. C*, in press.
54. P. Maris, private communication.
55. A. Bender, *et al.*, “Deconfinement at finite chemical potential”, nucl-th/9710069, *Phys. Lett. B*, in press.
56. R. T. Cahill and C. D. Roberts, *Phys. Rev. D* **32**, 2419 (1985).
57. D. Blaschke, C.D. Roberts and S. Schmidt, *Phys. Lett. B* **425**, 232 (1998).
58. G. Brown, *Nucl. Phys. A* **488**, 689c (1988).
59. P. Maris, C. D. Roberts and S. Schmidt, *Phys. Rev. C* **57**, R2821 (1998).
60. R. B. Wiringa, V. Fiks and A. Fabrocini, *Phys. Rev. C* **38**, 1010 (1988).
61. M. A. Pichowsky and T.-S. H. Lee, *Phys. Rev. D* **56**, 1644 (1997).
62. M. B. Hecht and B. H. J. McKellar, *Phys. Rev. C* **57**, 2638 (1998).
63. D. Klabucar and D. Kekez, “ $\eta$  and  $\eta'$  at the limits of applicability of a coupled Schwinger-Dyson and Bethe-Salpeter approach in the ladder approximation”: hep-ph/9710206.